Please cite this article in press as: Warren et al., Effects of polycationic drug carriers on the electromechanical and swelling properties of cartilage, Biophysical Journal (2022), https://doi.org/10.1016/j.bpj.2022.06.024

Biophysical Journal
Article

Biophysical Society

Effects of polycationic drug carriers on the electromechanical and swelling properties of cartilage

Matthew R. Warren,[1] Armin Vedadghavami,[1] Sanjana Bhagavatula,[1] and Ambika G. Bajpayee[1,2,*]
[1]Department of Bioengineering, Northeastern University, Boston, Massachusetts and [2]Department of Mechanical Engineering, Northeastern University, Boston, Massachusetts

ABSTRACT Cationic nanocarriers offer a promising solution to challenges in delivering drugs to negatively charged connective tissues, such as to articular cartilage for the treatment of osteoarthritis (OA). However, little is known about the effects that cationic macromolecules may have on the mechanical properties of cartilage at high interstitial concentrations. We utilized arginine-rich cationic peptide carriers (CPCs) with varying net charge (from +8 to +20) to investigate the biophysical mechanisms of nanocarrier-induced alterations to cartilage biomechanical properties. We observed that CPCs increased the compressive modulus of healthy bovine cartilage explants by up to 70% and decreased the stiffness of glycosaminoglycan-depleted tissues (modeling OA) by 69%; in both cases, the magnitude of the change in stiffness correlated with the uptake of CPC charge variants. Next, we directly measured CPC-induced osmotic deswelling in cartilage tissue due to shielding of charge repulsions between anionic extracellular matrix constituents, with magnitudes of reductions between 36 and 64 kPa. We then demonstrated that electrostatic interactions were required for CPC-induced stiffening to occur, evidenced by no observed increase in tissue stiffness when measured in hypertonic bathing salinity. We applied a non-ideal Donnan osmotic model (under triphasic theory) to separate bulk modulus measurements into Donnan and non-Donnan components, which further demonstrated the conflicting charge-shielding and matrix-stiffening effects of CPCs. These results show that cationic drug carriers can alter tissue mechanical properties via multiple mechanisms, including the expected charge shielding as well as a novel stiffening phenomenon mediated by physical linkages. We introduce a model for how the magnitudes of these mechanical changes depend on tunable physical properties of the drug carrier, including net charge, size, and spatial charge distribution. We envision that the results and theory presented herein will inform the design of future cationic drug-delivery systems intended to treat diseases in a wide range of connective tissues.

SIGNIFICANCE Osteoarthritis is a burdensome, highly debilitating degenerative joint disease that affects millions of people worldwide. Clinical translation of disease-modifying osteoarthritis drug candidates has been difficult, due in part to challenges in delivering therapeutic compounds to articular cartilage. Positively charged drug nanocarriers offer a promising solution for efficient intra-cartilage delivery. However, little is known about how these potential treatments interact with cartilage tissue, which may lead to altered mechanical properties. This is a crucial consideration for designing cationic delivery molecules, since it is imperative to avoid further exacerbation of the already compromised mechanical integrity of arthritic cartilage. Here, we evaluate the effects of positively charged peptide delivery systems on cartilage biomechanics and elucidate biophysical carrier-tissue matrix interactions that mediate these changes.

INTRODUCTION

Currently, there is no Food and Drug Administration-approved, disease-modifying treatment available for osteoarthritis (OA). Although numerous preclinical compounds such as glucocorticoids (1) and protein growth factors (2) have shown promising anti-catabolic and regenerative activity in connective tissues, their clinical translation has proved challenging, due in part to the difficulty of delivering drugs to articular cartilage (3,4). Cartilage is an aneural, avascular tissue composed of a dense meshwork of structural type II collagen and heavily glycosylated, anionic aggrecan proteoglycans (5,6). As such, systemic injections are ineffective in targeting cartilage, and drugs face significant steric

Submitted January 5, 2022, and accepted for publication June 23, 2022.
*Correspondence: a.bajpayee@northeastern.edu
Editor: Alex Mogilner.
https://doi.org/10.1016/j.bpj.2022.06.024

Please cite this article in press as: Warren et al., Effects of polycationic drug carriers on the electromechanical and swelling properties of cartilage, Biophysical Journal (2022), https://doi.org/10.1016/j.bpj.2022.06.024

hindrance and rapid clearance from the joint space following an intra-articular (IA) injection (3). As a potential solution, the strategy of charge-mediated intra-cartilage drug delivery has been introduced and developed over the past decade (7,8). This delivery modality leverages attractive electrostatic interactions between high valency, positively charged macromolecular carriers, and the negative fixed charge density (FCD) of glycosaminoglycan (GAG) chains in cartilage, which enables spontaneous partitioning into the interstitial space of the tissue's extracellular matrix (ECM) following an IA injection (9). By this mechanism, the dense cartilage ECM is effectively transformed into a drug depot, facilitating therapeutically effective intra-cartilage exposure levels to chondrocyte targets deep within the tissue (10,11). Multiple variations of peptide-based (12,13), protein-based (14–17), polymer-based (18–20), and particle-based (21) cationic constructs have proved effective in rapidly penetrating the full thickness of cartilage tissue; however, the effects of such nanocarriers on the electro-mechano-chemical homeostasis of cartilage (due to their high molecular weight and multivalent cationic charge) have yet to be thoroughly evaluated (22,23). This is a crucial consideration, since perturbations to this balance in vivo could compromise the tissue's ability to withstand physiological loads. Not only is it essential to evaluate the adverse effects of cationic drug carriers on the mechanical properties and biological health of cartilage (7,21,24), but a mechanistic understanding of the biophysical interactions underlying such changes in relation to the physical features of the drug-delivery system (DDS) will also inform the design of future cationic carriers.

The primary function of articular cartilage is to facilitate smooth joint motion by 1) providing a low-friction surface for joint articulation and 2) acting as a dynamic shock absorber between bone ends (25,26). As such, the functionality of cartilage is crucially dependent on its shear and compressive mechanical strength. The mechanical properties of cartilage arise from the fine electro-mechano-chemical balance between its macromolecular matrix constituents. Under triphasic theory (27), cartilage tissue is composed of three physical phases that contribute to its mechanical integrity: the solid collagen/proteoglycan ECM, interstitial fluid (which can be pressurized under non-equilibrium loading), and charged small ions/polyelectrolytes (i.e., Na^+, GAGs) dispersed throughout the interstitium (28). Importantly, since anionic GAG chains are interspaced along core proteins by a distance similar to their Debye length (29), like-charge Coulombic repulsion between neighboring chains confers significant resistance to compressive forces at the macro scale (30,31). This electrostatic/Donnan component of the tissue's mechanical strength augments the integrity provided by the macromolecular solid matrix (i.e., the non-Donnan component), and previous estimates have attributed up to 62% of cartilage's equilibrium compressive modulus to GAG-associated charge repulsions (32). Furthermore, GAG repulsions also provide the tissue with a free swelling pressure, which exists in equilibrium with constraining tensile forces from collagen fibers (33,34); therefore, cartilage is prestressed even at rest.

Considering the intimate dependence of cartilage biomechanical properties on the delicate physical relationships between the various ECM components, perturbations to this balance by high interstitial concentrations of a cationic DDS could have consequences for the tissue's mechanical functionality. For instance, due to their polyelectrolyte nature, the intra-tissue counter charge introduced by a cationic DDS may intuitively be expected to mask repulsive forces between GAG chains. Intra-cartilage charge shielding by small counterionic species (Na^+) at high concentrations is a well-characterized phenomenon that is known to induce significant deswelling and loss of compressive strength (35–37); as such, the free swelling pressure and modulus of cartilage are highly dependent on the osmotic environment. Our group has previously hypothesized that cationic drug carriers may induce a similar charge-shielding effect, and we recently developed a Donnan-equilibrium osmotic model to predict the reductions in swelling pressure and modulus associated with empirically observed uptake concentrations of differentially charged cationic peptides (23). However, the theoretically predicted phenomenon of carrier-induced charge shielding has yet to be empirically validated. Moreover, a macromolecular, multivalent cationic DDS may be expected to interact extensively with ECM constituents (such as anionic proteoglycans) through non-specific binding interactions (5,12), and it is unknown whether such interactions can facilitate additional confounding effects on the mechanical properties of the tissue.

Our group has designed and characterized cationic peptide carriers (CPCs) for optimal penetration and retention of therapeutics in articular cartilage (12,38). CPCs are 3 kDa, $\approx$20-amino-acid, α-helical peptides consisting of cationic arginine residues interspaced with alanine units for charge separation. CPCs rely on long-range electrostatic attractive forces as well as synergistic short-range hydrophobic interactions (via alanine residues) and hydrogen bonding for rapid penetration through cartilage and retention on the order of days (12). Given the ease of altering their primary amino acid sequence, CPCs are a highly modular delivery system, with readily tunable net charge, length, and spatial distribution of cationic residues. Our group has leveraged this versatility by synthesizing CPCs with varying net charge (from +8 to +20) and equal size, which has enabled systematic characterization of the influence of the carrier's charge, spatial charge distribution, and hydrophobicity on intra-cartilage transport properties. In the current study, we aimed to utilize CPCs in a similar manner as an experimental tool. The differential charge and equilibrium uptake levels of CPC variants allow us to directly probe the relationship between these properties and the mechanical response in cartilage. Further, the strong

Please cite this article in press as: Warren et al., Effects of polycationic drug carriers on the electromechanical and swelling properties of cartilage, Biophysical Journal (2022), https://doi.org/10.1016/j.bpj.2022.06.024

binding capacity of CPCs with ECM constituents also enables investigation of mechanical effects resulting from carrier-solid matrix interactions, beyond charge shielding.

The goal of this study was to use CPCs to investigate alterations to the mechanical properties of articular cartilage associated with the uptake of cationic DDS, with a focus on elucidating the biophysical mechanisms underlying such changes. We hypothesized that, in addition to shielding of like-charge repulsions of neighboring GAGs, the multivalency and distance between charged moieties across the peptide length may facilitate interactions with macromolecular constituents of the cartilage ECM that could also lead to downstream changes in compressive mechanical properties. Using stress-relaxation, dynamic, and osmotic mechanical testing, we measured the relationship between the physical properties of CPCs (i.e., net charge and uptake) and the equilibrium and fluid flow-dependent mechanical behavior of tissue explants with variable FCD. Next, we adapted our previously described Donnan osmotic model to deconvolute bulk equilibrium mechanical measurements into Donnan and non-Donnan components, which allowed us to probe the biophysical interactions underlying observed CPC-induced mechanical changes. Finally, we evaluated the implications of such perturbations on the tissue's health by utilizing in vitro chondrocyte and cartilage explant culture systems to measure the biological response to CPCs. In addition to providing a critical evaluation of CPCs individually as a potential clinically translatable intra-cartilage DDS, we envision that the principles of carrier-ECM biophysical interactions elucidated herein can inform the design of future cationic DDS.

MATERIALS AND METHODS

Materials

Phosphate-buffered saline (PBS), salts, and other reagents were purchased from Sigma (St. Louis, MO). Protease Inhibitor Mini Tablets were obtained from Thermo Fisher Pierce (Rockford, IL). Proteinase-K was from Roche Diagnostics (Risch-Rotkreuz, Switzerland). Tissue medium components were purchased from the following suppliers: Dulbecco's modification of Eagle's medium (DMEM) from Cellgro (Manassas, VA); HEPES, insulin-transferrin-selenium (ITS), trypsin-EDTA, penicillin-streptomycin antibiotic-antimycotic (PSA), and non-essential amino acids (NEAA) from Gibco (Carlsbad, CA); ascorbic acid and L-proline from Fisher Bioreagents (Pittsburgh, PA). Propidium iodide was purchased from Thermo Fisher Acros Organics (Geel, Belgium), and fluorescein diacetate (FDA) was obtained from Sigma (St. Louis, MO).

Cartilage explant preparation

Bovine articular cartilage explants were harvested as previously described (12,39). Full-thickness, 3-mm-diameter cartilage plugs were punched from the femoropatellar groove of 2-week-old bovine calf knee joints, purchased from a local slaughterhouse (Research 87, Boylston, MA). Plugs were sliced to produce 1-mm-thick cartilage disks with intact superficial zone. Disks were washed and equilibrated in PBS supplemented with PSA for 1 h and then stored at −20°C in PBS supplemented with protease inhibitor (PBS-PI) until experimentation. To prepare GAG-depleted cartilage disks as a model for mid-stage OA, explants were incubated in 0.1 mg/mL trypsin-EDTA in PBS at 37°C for 4 h, followed by a 1-h wash in PBS-PI. Following mechanical experiments, explants were digested by overnight proteinase-K incubation, and GAG content in the tissue lysate and surrounding bath from trypsin digestion was measured by dimethyl-methylene blue (DMMB) assay (40).

Cationic peptide preparation and equilibrium uptake into cartilage

Custom CPCs of various net charge (+8, +14, +16, and +20) conjugated to 6-carboxyfluorescein (FAM) were synthesized by Fmoc solid-phase peptide synthesis as previously described (12). Peptides of desired size and charge were designed by manipulating the number of arginine residues and utilizing alanine residues as spacers for even spatial charge distribution along the peptide length. See Table 1 for a summary of CPC sequences.

CPC solution for cartilage uptake experiments was prepared by reconstituting FAM-labeled CPCs in PBS-PI to a final concentration of 30 μM. For equilibrium uptake experiments, individual cartilage disks were incubated in 300 μL of CPC solution in a 96-well plate for 24 h at 37°C with light shaking. Cartilage explants were subsequently stored at −20°C in PBS-PI until mechanical testing. Following CPC absorption, the FAM fluorescence in the surrounding bath was measured at 490/525 nm using a microplate reader (Synergy H1; BioTek, Winooski, VT); fluorescence measurements were converted to concentration using a linear standard curve of known concentrations of CPC in PBS-PI. Total CPC uptake into individual explants was calculated as the ratio between the concentration of CPC absorbed into the tissue and the CPC concentration remaining in the surrounding bath following the 24-h absorption; that is,

$$R_U = \frac{\overline{C}_{CPC}}{C_{CPC}}, \tag{1}$$

where R_U is the CPC uptake ratio, $\overline{C}_{CPC}$ is the intra-cartilage CPC concentration (per intra-tissue water volume), and C_{CPC} is the concentration of CPC in the surrounding bath after 24 h of uptake.

Stress-relaxation mechanical testing

The equilibrium stiffness of tissue explants pre-equilibrated with CPC was measured by uniaxial, unconfined, stress-relaxation testing on a TA ElectroForce 5500 Series dynamic mechanical analysis apparatus (TA Instruments, New Castle, DE). An unconfined setup was chosen for mechanical tests because: 1) it allows for a larger bath-explant interface during CPC diffusion; 2) radial CPC diffusion during tests eliminates depth-dependent anisotropy in axial solute penetration; and 3) a porous platen was not required, minimizing the surface area of the bath-stainless steel interface, to which CPCs may bind non-specifically. The testing setup consisted of a 15-mm-diameter stainless steel chamber mounted atop a TA ElectroForce 50 lbf load cell. Samples were compressed with a flat, stainless steel, 10-mm-diameter cylindrical platen controlled by a motor according to a preset movement process on WinTest software (TA Instruments). Load and platen displacement data were acquired and recorded by the software every 0.05 s.

TABLE 1 Charged peptide carrier (CPC) net charge, sequence, and size

CPC net charge (z)	Amino acid sequence	Peptide size (Da)
+8	$(RRAAAA)_3RR$	2478.7
+14	$RRRR(AARRR)_3R$	2989.3
+16	$(ARRRAARA)_4$	4012.4
+20	$(RRRRR)_4$	3500.0

R, arginine; A, alanine.

Please cite this article in press as: Warren et al., Effects of polycationic drug carriers on the electromechanical and swelling properties of cartilage, Biophysical Journal (2022), https://doi.org/10.1016/j.bpj.2022.06.024

Prior to testing, frozen explants were thawed and equilibrated in PBS-PI at 37°C for 15 min. The thickness of each cartilage disk was measured at multiple locations using calipers. Disks were placed at the bottom of the testing chamber with the deep zone of the disk down, in contact with the bottom of the well, such that the superficial zone was probed during testing. The well was then filled with 800 μL of 0.15 M (1×) PBS, and the sample was equilibrated with the bathing solution for 5 min. A preload of 0.1 N was then applied to the tissue to ensure platen contact, followed by an 800 s equilibration period at constant strain. The sample was then subjected to successive compressive strain ramps of 4%, 2%, and 2% (reaching 8% cumulative strain), applied at a rate of 0.0001 mm/s, with each ramp followed by an 800 s dwell period, which was confirmed to be adequate for the tissue to reach an equilibrium stress after the applied strain.

Cyclic loading

Immediately following the final strain hold of stress-relaxation testing, explants from all CPC treatment conditions were subjected to dynamic mechanical testing, consisting of two rounds of sinusoidal compressive loading (41). Explants underwent testing at two frequencies: 0.01 Hz, at which sufficient time is given for fluid flow through the tissue with low dissipative drag ($1/f \approx \tau$) (42); and 1 Hz, to mimic loading rates typically experienced during walking. Following a 600 s equilibration at 8% strain at the end of stress relaxation, cyclic strain was initiated at 0.01 Hz with an amplitude of $\pm$0.5% (superimposed on the 8% baseline strain) for 30 cycles, and the resultant stress response was recorded. Immediately after the 0.01 Hz test, the tissue was allowed to relax for 600 s and subsequently was subjected to 30 cycles of $\pm$0.5% strain at 1 Hz.

Real-time measurement of CPC-induced stress reduction

Intra-tissue stress during and immediately after transient CPC uptake was measured using a testing method and model based on the technique described by Eisenberg and Grodzinsky (36). Native cartilage disks (not pretreated with CPC) were thawed at 37°C and allowed to equilibrate in PBS-PI for 15 min. Next, explants were transferred to hypotonic PBS (0.015 M, or 0.1×) and incubated for 40 min at room temperature for equilibration. Disks were then placed at the bottom of the testing chamber, and 600 μL of 0.015 M (0.1×, hypotonic) PBS was added to the well. Hypotonic PBS was used such that osmotic pressure changes with higher magnitude (and higher signal/noise ratio) would be observed due to higher overall tissue swelling. A preload of 0.07–0.1 N was then added to the disk to ensure platen contact. The sample was equilibrated to the preload at constant strain for 1000 s, which was then followed by five successive ramp/dwell cycles of $\approx$2% compressive strain held for 800 s each. After the fifth ramp/dwell cycle, a small volume ($\approx$50 μL) of concentrated CPC was added to the testing well to a final concentration of 30 μM. The resultant drop in stress in the tissue throughout CPC uptake was measured by holding a constant strain for 2 h and recording stress measurements every 0.05 s. After the equilibration period, the disk was subjected to four reverse ramp/dwell cycles of $\approx$1% strain, held for 1000 s each.

Stress-relaxation testing with varying salt concentration

For multi-salt concentration tests, explants were first prepared by 24-h equilibration with either PBS-PI or 30 μM CPC +14 as described above (see cationic peptide preparation and equilibrium uptake into cartilage). For experimentation, frozen explants were thawed for 20 min at 37°C and subsequently allowed to equilibrate in 0.02 M NaCl for 40 min at room temperature. Following this period, explants were loaded on the mechanical testing apparatus as described above with an 800 μL bath of 0.02 M NaCl. A preload of 0.1 N was then added to ensure platen contact with the explant surface, and the tissue was equilibrated to the preload for 1000 s.

The testing process consisted of five consecutive sets of stress-relaxation tests, each at a different salt concentration (0.02 M, 0.07 M, 0.19 M, 0.6 M, and 1.4 M; measured by a freezing point osmometer (34)). The first stress-relaxation test (at hypotonic saline, or 0.02 M) consisted of a $\approx$4% strain ramp, followed by a 2000 s hold for relaxation. After the first 1000 s (by which point equilibrium stress had been reached), a small volume (<100 μL) of concentrated NaCl was added to the testing bath and mixed thoroughly, such that the bath was now at the next salinity level (i.e., 0.07 M). The explant was then allowed to equilibrate to the new salt concentration at constant strain for 1000 s (the remaining time in the 2000 s strain hold), during which salt-induced stress relaxation occurred. After this period, a new set of stress relaxation was instigated, consisting of a negative $\approx$2% strain ramp/1000 s hold, followed by a positive $\approx$4% strain ramp (positive = compression). Negative strain ramps were used to avoid cumulative compression of the sample beyond 16% throughout the duration of the test. Finally, after the 4% strain ramp, another 2000 s hold was instigated so that the salt concentration could be changed again. This process was repeated for a total of four times after the initial 4% stress-relaxation test, such that stress relaxation was performed at five different salt concentrations. See Fig. S1 for a full depiction of the temporal stress and strain courses.

Mechanical data analysis

To extract mechanical parameters from raw data, temporal stress and strain data from all mechanical tests were analyzed in MATLAB.

Stress-relaxation analysis

For each explant, three separate stress-relaxation intervals were obtained throughout testing. To extract values for equilibrium stress and characteristic time constant, temporal stress data for each relaxation interval was separately fit to the standard linear solid (SLS) model using non-linear least-squares regression, in the following form (43):

$$\sigma(t) = \sigma_{eq} + \left(\sigma \times e^{-\frac{t}{\tau}}\right), \tag{2}$$

where σ is stress (Pa), σ_{eq} is the equilibrium stress (Pa), t is time (s), and τ is the tissue characteristic time constant (s); Since τ was extracted independently for each relaxation interval, it was measured in triplicate and averaged for each sample. Subsequently, the equilibrium modulus (E_{eq}) for the tissue was calculated as the slope of the linear regression of the resultant equilibrium stress-strain relationship. Using E_{eq} and τ, the permeability (K) of each sample was estimated following the biphasic poroelastic model described by Mow and colleagues (44), using the formula

$$K \propto \frac{L^2}{E_{eq} \times \tau}, \tag{3}$$

where L is the radius of each disk (1.5 mm), signifying the distance over which fluid flows out of the tissue during unconfined compression. Since the mechanical parameters used to estimate permeability were extracted from a solid viscoelastic (SLS) model, permeability values reported here were normalized to control (see Fig. S2).

Dynamic loading analysis

For each oscillatory loading frequency tested, the temporal stress and corresponding strain data were fit to a sinusoidal function in the following form:

$$\sigma(t) = A_{stress} \times \cos(2\pi f t + \theta_{stress}), \tag{4}$$

Please cite this article in press as: Warren et al., Effects of polycationic drug carriers on the electromechanical and swelling properties of cartilage, Biophysical Journal (2022), https://doi.org/10.1016/j.bpj.2022.06.024

$$\varepsilon(t) = A_{strain} \times \cos(2\pi ft + \theta_{strain}), \quad (5)$$

where t is time (s), A_i is the amplitude of the waveform (Pa), θ_i is the phase angle of the waveform (in rad, relative to $t = 0$), and f is the frequency (either 0.01 Hz or 1 Hz). Thus, four sinusoidal functions were obtained for each explant, one describing stress and one describing strain as a function of time for both 0.01 Hz and 1 Hz. From these fits, two mechanical parameters were obtained at each frequency (45): the dynamic modulus G^* (Pa) and the relative phase shift θ (deg) between the stress and strain waves. These values were calculated using the following formulas:

$$G^* = \frac{A_{stress}}{A_{strain}}, \quad (6)$$

$$\theta = \frac{-180}{\pi} \times (\theta_{strain} - \theta_{stress}). \quad (7)$$

Osmotic swelling pressure analysis

In applying the testing methodology described by Eisenberg and Grodzinsky (36), the macroscale, equilibrium mechanical behavior of cartilage is described by a modified Hooke's law of the following form, relating equilibrium stress (σ_{eq}) to strain (ε_0):

$$\sigma_{eq} = \left[E_{eq}(\overline{C}, z) \times \varepsilon_0\right] + \beta(\overline{C}, z). \quad (8)$$

In this constitutive equation, both the Young's modulus E_{eq} and chemical stress β are assumed to depend on the intra-tissue concentration of the charged species under consideration ($\overline{C}$) and the net charge of that species (z). Importantly, the tissue chemical stress β is defined as follows. When a tissue sample is at equilibrium with a bath of sufficient ionic strength to shield all charge interactions between matrix constituents, there is zero tissue swelling due to electrical repulsive forces, and the sample remains at a baseline reference thickness. Upon decreasing the bath ionic concentration to a given level, small counterions (i.e., Na^+) diffuse from the tissue space and matrix GAG charge repulsions arise, increasing the thickness of the tissue. At a given ionic concentration, β is defined as the stress that would need to be applied to return the tissue to the baseline reference thickness. β can alternatively be considered as the free swelling stress generated by intra-tissue charge repulsions, equal to σ_{eq} at zero tissue strain ($\varepsilon_0 = 0$ in Eq. 8).

Temporal stress data from swelling pressure tests (see real-time measurement of CPC-induced stress reduction) was first separated into two portions: the five initial stress/relaxation cycles before the addition of CPC, and the four reverse stress/relaxation cycles after the long static hold following CPC addition. Each of these data sets were analyzed as a separate stress-relaxation test as described above (stress-relaxation analysis): individual relaxation intervals were isolated and fit to the SLS model, and two separate sets of equilibrium stress-strain values were extracted for each cartilage explant tested. These data were then fit to Eq. 8 by linear regression, and both a pre- and post-CPC slope and y-intercept were obtained. Importantly, in fitting Eq. 8 to the data, β is represented by the y-intercept, since $\sigma_{eq} = \beta$ at $\varepsilon_0 = 0$. Therefore, the magnitude of the change in chemical stress due to CPC was calculated as the difference in y-intercept between the two stress/strain curves obtained; that is,

$$\Delta\beta = \beta_{CPC} - \beta_{PBS}. \quad (9)$$

Notably, by the calculation method herein, the chemical stress within the tissue is set to be zero at hypotonic salinity. Thus, CPC-associated deswelling is quantified as the magnitude of the resultant drop in chemical stress relative to the hypotonic chemical stress, and a higher drop in stress represents more charge shielding by the CPC.

Multi-concentration test analysis

For data obtained from stress-relaxation testing at multiple salt concentrations, individual stress-relaxation intervals were isolated and fit to the SLS model to extract equilibrium stress values, as described above in stress-relaxation analysis. Stress values were plotted against corresponding strain levels (calculated relative to a hypertonic reference thickness), and five stress-strain data sets were obtained (one for each salinity level). These data sets were each then fit to a linear regression model, and measurements for equilibrium Young's modulus at each salt concentration were obtained as the slope of the corresponding linear fit. See Fig. S1 for a depiction of the data analysis technique used for multi-salinity testing data.

Non-ideal Donnan modeling of osmotic swelling pressure

We aimed to generate estimates for free swelling pressures and electrostatic/Donnan moduli in cartilage based on CPC uptake and GAG content measurements. A modified Donnan osmotic model was used as previously described by our group (23), which incorporates the counter charge introduced by intra-tissue CPC into the electroneutrality condition of the classical Donnan framework and thus accounts for deswelling induced by CPC charge shielding. Importantly, given the availability of empirical data from the experiments performed herein (intra-tissue CPC concentrations, GAG content, and Young's modulus at multiple salt concentrations), we were able to modify our previously published ideal Donnan model by using the non-ideal modeling approach described by Zimmerman et al. (34). This involves introducing an empirical attenuation parameter ξ as a scaling factor to the tissue's FCD, which is derived from classical counterion condensation theory (46,47). The equation used to calculate intra-tissue swelling pressures was the following, derived fully in the supporting material:

$$\pi_{FCD} = \alpha\Phi RT\left[\sqrt{\left[\xi\overline{C}_{FCD} + (z \times \overline{C}_{CPC})\right]^2 + 4C_0^2} - 2C_0\right], \quad (10)$$

where π_{FCD} is the swelling pressure (in kPa; the theoretical analog to the measured parameter β), Φ is the ion concentration-dependent, non-ideal osmotic coefficient, R is the universal gas constant, T is the temperature (293 K), z is the charge of the CPC, C_0 is the surrounding bath salinity (in M), $\overline{C}_{CPC}$ is the intra-tissue concentration of CPC, and $\overline{C}_{FCD}$ is the FCD of the tissue (in Eq/L). As previously described (23,30), this equation for swelling pressure was extended to calculate a component of the bulk Young's modulus of the tissue arising from like-charge repulsions (referred to as the "Donnan component" or E_{eq}^{Donnan}). In brief, this was done by expressing $\overline{C}_{FCD}$ and $\overline{C}_{CPC}$ as functions of tissue strain ϵ in accordance with a confined testing setup and calculating E_{eq}^{Donnan} using the relation $E_{eq}^{Donnan} = \frac{d}{d\varepsilon}(\pi_{FCD})$. To account for differences between the experimental setup used here and that described by Zimmerman et al. (i.e., unconfined versus confined compression setup), we have also included an extra scaling factor α in the equation to be fit with experimental data in addition to ξ.

Having defined a model for calculating E_{eq}^{Donnan} based on the measurable parameters $\overline{C}_{FCD}$, $\overline{C}_{CPC}$, z, and C_0, we next obtained empirical values for the unknown variables ξ and α. This was done by fitting the above model (E_{eq}^{Donnan} calculated from Eq. 10) to modulus measurements obtained at various C_0 with untreated control explants (see stress-relaxation testing with varying salt concentration). Under a triphasic framework at equilibrium, where fluid pressurization is zero, the bulk measurable compressive modulus of cartilage can be expressed as the sum of two components (30):

$$E_{eq}^{Meas} = E_{eq}^{Donnan} + E_{eq}^{Non-Donnan}, \quad (11)$$

where E_{eq}^{Meas} is the measured modulus and $E_{eq}^{Non-Donnan}$ is the component of the modulus arising from support by the solid macromolecular ECM (referred to as

Please cite this article in press as: Warren et al., Effects of polycationic drug carriers on the electromechanical and swelling properties of cartilage, Biophysical Journal (2022), https://doi.org/10.1016/j.bpj.2022.06.024

the "non-Donnan component"). In fitting the Donnan model to experimental data, we applied the assumption that for untreated cartilage, $E_{eq}^{Non-Donnan}$ is independent of the surrounding salt concentration in the bath. Another assumption made was that the Donnan component E_{eq}^{Donnan} is zero at sufficiently high salt concentrations, such that the FCD of the tissue is completely masked. Under these assumptions, $E_{eq}^{Non-Donnan}$ (at all C_0) is equal to the bulk modulus E_{eq}^{Meas} measured at hypertonic salinity (i.e., 1.4 M, see stress-relaxation testing with varying salt concentration). Therefore, by subtracting this assumed value for $E_{eq}^{Non-Donnan}$ from E_{eq}^{Meas} across all concentrations, we were able to extrapolate empirical E_{eq}^{Donnan} values (by Eq. 11) at different C_0, for control explants. We then used non-linear regression to obtain fitted values for ξ and α with E_{eq}^{Donnan} data, with $\overline{C}_{CPC}$ and z set to zero. The non-ideal Donnan model fitted against E_{eq}^{Donnan} data across salt concentrations is shown in Fig. S3.

The empirical constitutive model for E_{eq}^{Donnan} was then applied in order to separate moduli measured across salt concentrations (from both untreated and CPC explants) into Donnan and non-Donnan components. Where available, explant-specific GAG content, wet weights, and intra-tissue CPC concentrations were used to generate modeling predictions for E_{eq}^{Donnan} for individual explants, which were averaged within treatment conditions. For experiments where GAG content/uptake ratios were not measured, representative average values from previous studies (12) were used.

Live explant culture

For live tissue studies, cartilage explant culture was instigated immediately after harvesting from bovine calf joints. The complete growth medium contained low-glucose DMEM, 1% HEPES buffer, 1% ITS, 1% NEAA, 1% ascorbic acid, and 0.4% proline (percentage of total volume). Prior to experimentation, explants were cultured for 48 h at 37°C and 5% CO_2. Explants were subsequently treated with medium containing 30 μM CPC for 48 h, followed by medium replacement with fresh, complete DMEM supplemented with CPC every 2 days for a total culture of 8 days post treatment. Following culture, explants were either digested with proteinase-K overnight for DMMB assay to quantify GAG loss or washed in PBS-PI for 1 h to prepare for cell viability assays.

Chondrocyte health

Chondrocyte metabolism was measured at the end of the 8-day culture via alamarBlue assay (BioRad, Hercules, CA). Immediately following culture, explant medium was replaced with complete DMEM containing the alamarBlue reagent. Tissues were subsequently incubated at 37°C for 3 h with protection from light. Explant medium was removed and fluorescence was read at 540/590 nm using a microplate reader.

Cell viability was assessed at the end of the 8-day culture by live-dead staining and imaging (39,43). On day 8 of the culture, thin explant sections were sliced and stained with 10 mg/mL propidium iodide and 4 mg/mL fluorescein diacetate (FDA) for 6 min. This mixture selectively stains non-viable cells red (by propidium iodide) and viable cells green (by FDA). Following staining, cartilage sections were washed with PBS and imaged at 4× magnification using an Eclipse Ts2R fluorescence microscope (Nikon, Tokyo, Japan). Separate live/dead images were overlaid using ImageJ software.

CPC uptake into chondrocytes

Primary chondrocytes were isolated from articular cartilage slices from bovine calf joints and cultured as previously described (48). Healthy chondrocyte monolayers were exposed to CPC peptides (+8 to +20) at a concentration of 5 μM for 1 h. After uptake, cells were washed twice with cold PBS and fixed for 10 min in 4% paraformaldehyde. Cell nuclei were stained with 4′,6-diamidino-2-phenylindole for 5 min. Cells were then imaged on a Nikon Eclipse Ts2R fluorescence microscope with constant exposure time. Images were processed with ImageJ software. To quantify uptake, cells were analyzed with a Cytoflex flow cytometer (Beckman Coulter, Brea, CA). CPC-associated fluorescence was measured with the fluorescein isothiocyanate channel, and 10,000 cell events were captured per sample.

Statistical analysis

All data presented herein represent mean ± standard deviation unless otherwise stated; where noted, 95% confidence intervals were calculated with the bootstrap method as previously described (49). In general, all experiments were conducted using $N = 3$–5 replicate explants in multiple experimental repeats with explants harvested from at least two different animals. Unless otherwise stated, for data sets with single comparisons only, statistical significance between means compared with control was determined using a two-way heteroscedastic Student's t-test, with $p \leq 0.05$ being considered significant. To correct for multiple comparisons, one-way ANOVA followed by Dunnett's post hoc test was used where appropriate.

RESULTS

The goal of this study was to investigate the effect of cationic DDS on the mechanical properties of articular cartilage. We utilized 3 kDa, ≈20-amino-acid CPCs with varying net positive charge to systematically probe the dependence of tissue-carrier interactions on the net charge and uptake of the carrier. Since the transport and equilibrium uptake properties of CPCs have been studied extensively (12,38), these molecules serve as an ideal experimental tool for mechanistic studies of the biophysical interactions underlying changes in tissue mechanical properties following treatment.

CPC uptake alters equilibrium and time-dependent mechanical properties of healthy and GAG-depleted cartilage

We first measured the modulus of cartilage explants following equilibrium uptake of CPCs with varying levels of net charge (+8 to +20) using stress-relaxation testing (Fig. 1, *A* and *B*). Goodness of fit to the SLS model (Eq. 2) was confirmed by calculating residual standard error, which, on average, was approximately 576 Pa for healthy explants and 370 Pa for GAG-depleted explants (less than 5% of the magnitude of stress measurements). In general, the equilibrium modulus increased following uptake of CPC in tissue samples with native FCD (Fig. 1 *C*). Explants treated with CPC +14 exhibited the highest increase in stiffness compared with untreated explants (399 kPa versus 235 kPa for CPC +14 and control, respectively, or a 69% increase). Notably, treatment with CPCs of higher net charge did not result in a larger stiffness increase: CPC +16 resulted in a modulus of 351 kPa (49% increase compared with control), and CPC +20 did not increase stiffness with statistical significance.

Additionally, cartilage explants with ≈50% FCD (mimicking mid-stage OA) were prepared via controlled tryptic digestion and mechanically probed following equilibrium CPC uptake. All modulus measurements for GAG-depleted explants were lower than normal-FCD explants

Please cite this article in press as: Warren et al., Effects of polycationic drug carriers on the electromechanical and swelling properties of cartilage, Biophysical Journal (2022), https://doi.org/10.1016/j.bpj.2022.06.024

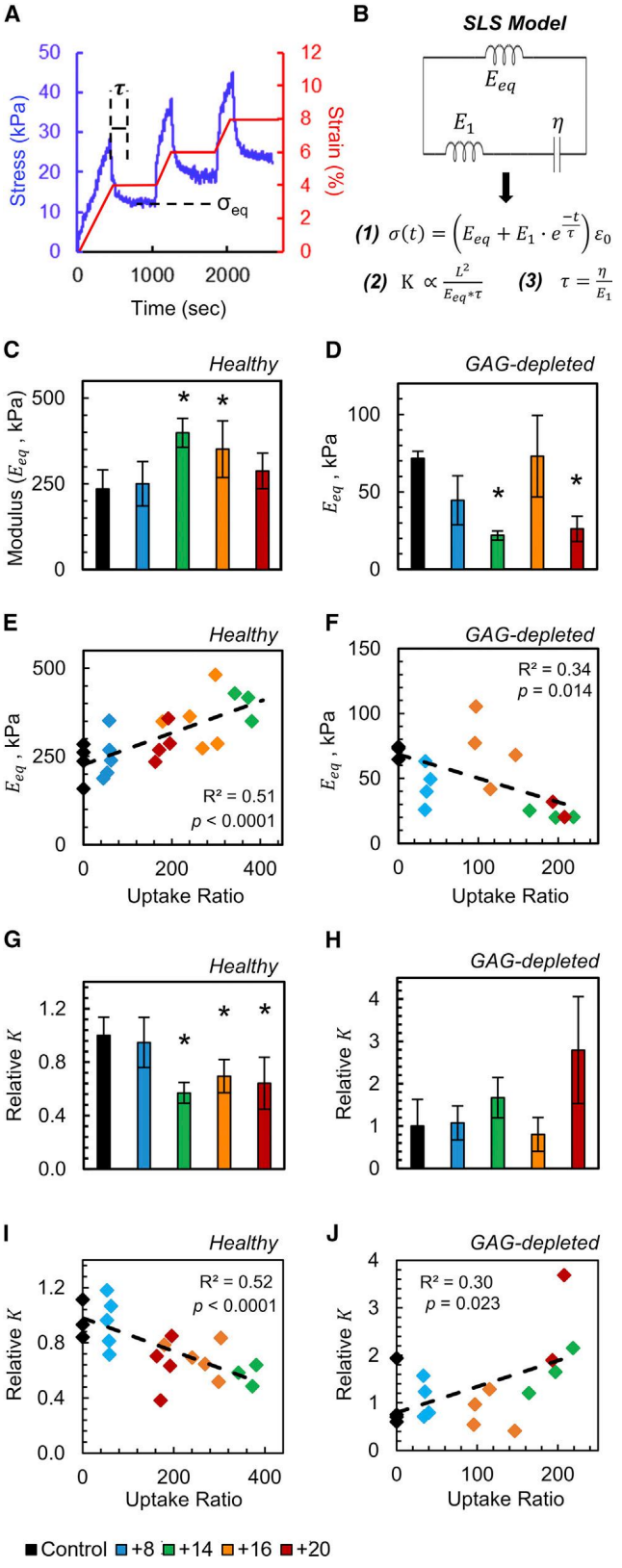

FIGURE 1 Stress-relaxation testing on normal-FCD and GAG-depleted cartilage explants, pre-equilibrated with CPC. (*A*) Depiction of the uniaxial, unconfined stress-relaxation testing process used to measure tissue characteristic time constant (τ) and equilibrium stress (σ_{eq}) at varying strains. (*B*) The standard linear solid (SLS) model was fit to individual stress-relaxation curves (three per test) to calculate equilibrium Young's modulus (E_{eq}) and permeability (K) from temporal mechanical data. (*C* and *D*) Equilibrium modulus of normal-FCD and 50% GAG-depleted explants, respectively, equilibrated with CPC of varying net charge (+8 to +20; see legend at bottom of figure). GAG-depleted explants modeling mid-state OA were prepared by trypsin digestion. (*E* and *F*) Correlation of equilibrium modulus with CPC uptake ratios for normal and GAG-depleted explants, respectively. (*G* and *H*) Measurements of hydraulic permeability of normal-FCD and GAG-depleted explants, respectively, relative to control; correlations between permeability and uptake are shown in (*I*) and (*J*). All data are presented as bars are means, with error bars representing standard deviations. Data points in correlation plots represent individual sample measurements. Statistical markers (*) represent $p \leq 0.05$ compared with control. $N = 3$–5 per condition; $N = 2$ for CPC +20, 50% GAG-depleted condition.

(235 kPa versus 71.6 kPa for normal and GAG-depleted control explants, respectively), as expected for tissues with lower FCD, with reductions similar to those in previous reports (50,51). Interestingly, an opposite trend with CPC treatment was observed in 50% GAG-depleted tissue compared with healthy cartilage: CPCs resulted in markedly decreased stiffness of the tissue (Fig. 1 *D*). Variants CPC +14 and CPC +20 resulted in a statistically significant decrease in modulus, −69%, and −63%, respectively compared with untreated control. This is in stark contrast to the observed stiffening in healthy tissues, suggesting that following CPC treatment multiple nanoscale biophysical phenomena may occur simultaneously within the tissue that depend on the properties of the ECM.

To further explore these contradictory observations and gain mechanistic insight, we plotted modulus measurements against CPC uptake ratio for each individual sample tested in both the normal-FCD and GAG-depleted experimental groups. As shown in Fig. 1, *E* and *F*, we observed a clear correlation between CPC uptake and stiffness in both types of cartilage (R^2 of 0.51 and 0.34 for normal-FCD and GAG-depleted, respectively). Notably, opposite trends were again observed between normal and GAG-depleted tissues: while higher uptake was correlated with increased tissue stiffness in healthy tissues, GAG-depleted tissues showed lower stiffness with higher uptake. These results provide further evidence that CPC molecules can interact with the cartilage ECM by multiple biophysical mechanisms, each of which depend on the amount of CPC within the tissue.

We next conducted further analysis of stress-relaxation data by extracting measurements for tissue hydraulic permeability (see stress-relaxation analysis (26) and Fig. S2 for further discussion of permeability calculations). Shown in Fig. 1, *G*–*J* are relative permeability estimates and respective correlations with CPC uptake for normal-FCD (Fig. 1, *G* and *I*) and GAG-depleted (Fig. 1, *H* and *J*) explants, normalized to control. For normal explants, CPC treatment resulted in decreased permeability, with CPC +14 showing the largest magnitude of decrease (by 43% compared with untreated control). CPCs +16 and +20 also showed statistically significant decreases in permeability, albeit to a lesser extent (by 30% and

Please cite this article in press as: Warren et al., Effects of polycationic drug carriers on the electromechanical and swelling properties of cartilage, Biophysical Journal (2022), https://doi.org/10.1016/j.bpj.2022.06.024

36%, respectively). Similar to modulus measurements, permeability correlated closely with CPC uptake—higher uptake resulted in lower permeability in healthy tissues ($R^2 = 0.52$). For GAG-depleted tissues, CPCs did not result in a significant change compared with control. Overall, the analysis of tissue permeability following CPC treatment provides further mechanistic insight into the interactions between CPC molecules and the cartilage ECM. The results suggest that macromolecular carriers can alter the time-dependent mechanical properties of cartilage, to an extent that depends on the amount of carrier within the tissue. This may arise either from hindered interstitial fluid flow and/or from increased friction between ECM macromolecules.

Pre-equilibrated healthy cartilage explants were also subjected to oscillatory compressive loading (Fig. 2 *A*). Two mechanical parameters were measured: the complex dynamic modulus G^* and the shift in phase angle θ between the strain and respondent stress waveforms. Considerably higher measurements for G^* were observed at the 1 Hz testing frequency, as expected due to increased pressurization of interstitial fluid at higher loading rates (45). For both testing frequencies, complex modulus measurements showed a trend similar to equilibrium modulus, albeit statistically insignificant: CPC uptake resulted in higher G^*, with a lesser magnitude than changes in equilibrium modulus (Fig. 2 *B*). Furthermore, minor (but statistically insignificant) alterations in the observed phase shift θ were measured in explants treated with CPC of higher net charge compared with control. These results suggest that despite large alterations to equilibrium mechanical stiffness, CPC-ECM interactions are not severe enough to induce changes to the tissue's mechanical response under physiological loading conditions. The mechanical properties measured herein are summarized in Table 2.

Charge shielding by intra-cartilage CPC induces osmotic deswelling within the tissue

Having observed contradictory effects of CPCs on tissue mechanical properties between healthy and GAG-depleted cartilage, we next aimed to further investigate the biophysical interactions between CPC molecules and matrix constituents that mediate these changes. We first hypothesized that the cationic charge introduced by intra-tissue CPCs can shield like-charge interactions between matrix proteoglycans (22,36). Since the compressive strength of cartilage relies heavily on electrostatic repulsion between neighboring anionic GAGs, we expect charge shielding by CPCs to considerably reduce the modulus of the tissue (as observed with GAG-depleted cartilage; Fig. 1 *D*) as well as the free osmotic swelling pressure (34).

We directly measured reductions in free swelling pressure induced by CPCs of varying net charge during and after real-time uptake. To measure swelling pressures (termed β), we adapted the testing protocol described by Eisenberg and Grodzinsky (36), in which stress is measured with a tissue sample under constant strain throughout the course of tissue equilibration with a surrounding counterionic solution (in this case CPC). The full testing process and data analysis technique are shown in Fig. 3, *A* and *B*; see the sections "real-time measurement of CPC-induced stress reduction" and "osmotic swelling pressure analysis" for an in-depth description of the process for measurement and quantification of swelling pressure reduction.

Fig. 3 *C* shows $\Delta\beta$ measurements for CPCs +8 through +20, taken using a 2 h CPC uptake time frame (hereby referred to as "transient" uptake, as CPC uptake has not reached equilibrium at 2 h). We measured considerable osmotic deswelling induced by CPC (between 36 and 64 kPa, or approximately 10%–20% of the tissue's modulus), which demonstrates the charge-shielding effect induced by intra-tissue CPC molecules. Notably, the magnitude of $\Delta\beta$ did not increase with CPC of higher net charge: while CPC +14 resulted in a −64.2 kPa drop, a considerably lower drop was observed in CPC +16 and +20 treatment groups (−43.7 kPa and −36.3 kPa, respectively). This may be reflective of the lower uptake of CPC +16 and +20 compared with CPC +14: as described by previous theoretical work (23), CPC charge shielding is expected to depend on both the net charge of the carrier and its

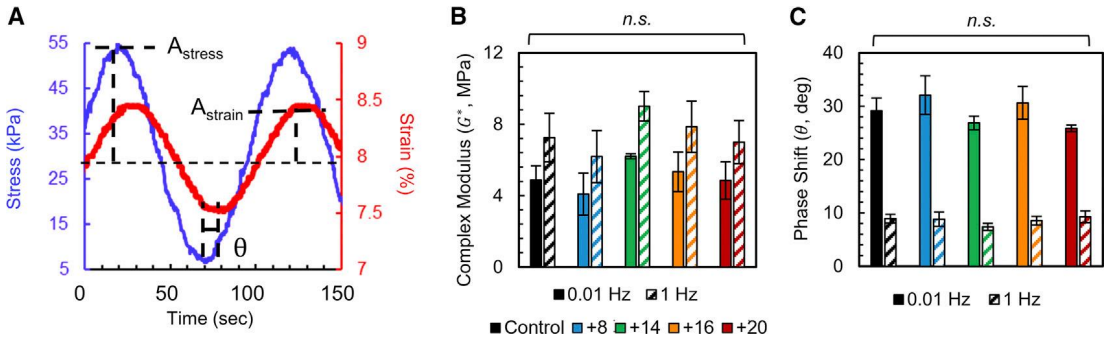

FIGURE 2 Dynamic mechanical testing on cartilage explants with normal FCD, pre-equilibrated with CPC. (*A*) Cartilage explants were subjected to sinusoidal strain waveforms (±0.5% amplitude at 0.01 and 1 Hz) to determine complex modulus (*B*) and phase shift (*C*) following treatment with CPCs carrying net charge. Data are plotted as means with error bars representing standard deviations. n.s., not significant.

Please cite this article in press as: Warren et al., Effects of polycationic drug carriers on the electromechanical and swelling properties of cartilage, Biophysical Journal (2022), https://doi.org/10.1016/j.bpj.2022.06.024

TABLE 2 Summary of measured CPC-associated mechanical and transport properties in healthy articular cartilage

	Control	CPC +8	CPC +14	CPC +16	CPC +20
Uptake ratio	N/A	55.6 ± 6.8	375.4 ± 26.4	258.0 ± 50.8	184.5 ± 14.9
Partitioning factor (k)	N/A	7.6	3.4	3.0	1.8
Equilibrium modulus (E_{eq}, kPa)	235 ± 55	250 ± 65	399 ± 43	351 ± 83	287 ± 52
Complex dynamic modulus ($G*$, MPa)					
0.01 Hz	4.9 ± 0.8	4.1 ± 1.2	6.2 ± 0.1	5.3 ± 1.1	4.8 ± 1.0
1 Hz	7.2 ± 1.4	6.2 ± 1.5	9.0 ± 0.8	7.9 ± 1.4	7.0 ± 1.2
Swelling pressure reduction ($\Delta\beta$, kPa)	N/A	−53.1 ± 23.3	−64.2 ± 9.9	−43.7 ± 12.6	−36.3 ± 7.7

Data are presented as mean ± standard deviation. CPC, cationic peptide carrier.

intra-tissue concentration. Here, lower transient uptake of CPCs +16 and +20 may have outweighed the higher net charge, resulting in a lower amount of total moles-charge being introduced into the tissue. These results therefore provide evidence that the magnitude of $\Delta\beta$ depends directly on CPC uptake in addition to net charge.

In addition to quantifying net $\Delta\beta$, we also considered the temporal course of stress reduction induced during real-time CPC uptake (i.e., from time $b \rightarrow c$). Fig. 3 *D* shows representative curves of stress reduction over time (under constant strain) in explants treated with each CPC variant. For comparison across samples, stress values were calculated relative to the stress measured at the time of CPC addition, which was defined as $t = 0$. Interestingly, deswelling did not occur at a constant rate over the 2-h uptake period. Rather, the temporal course of deswelling was largely reflective of

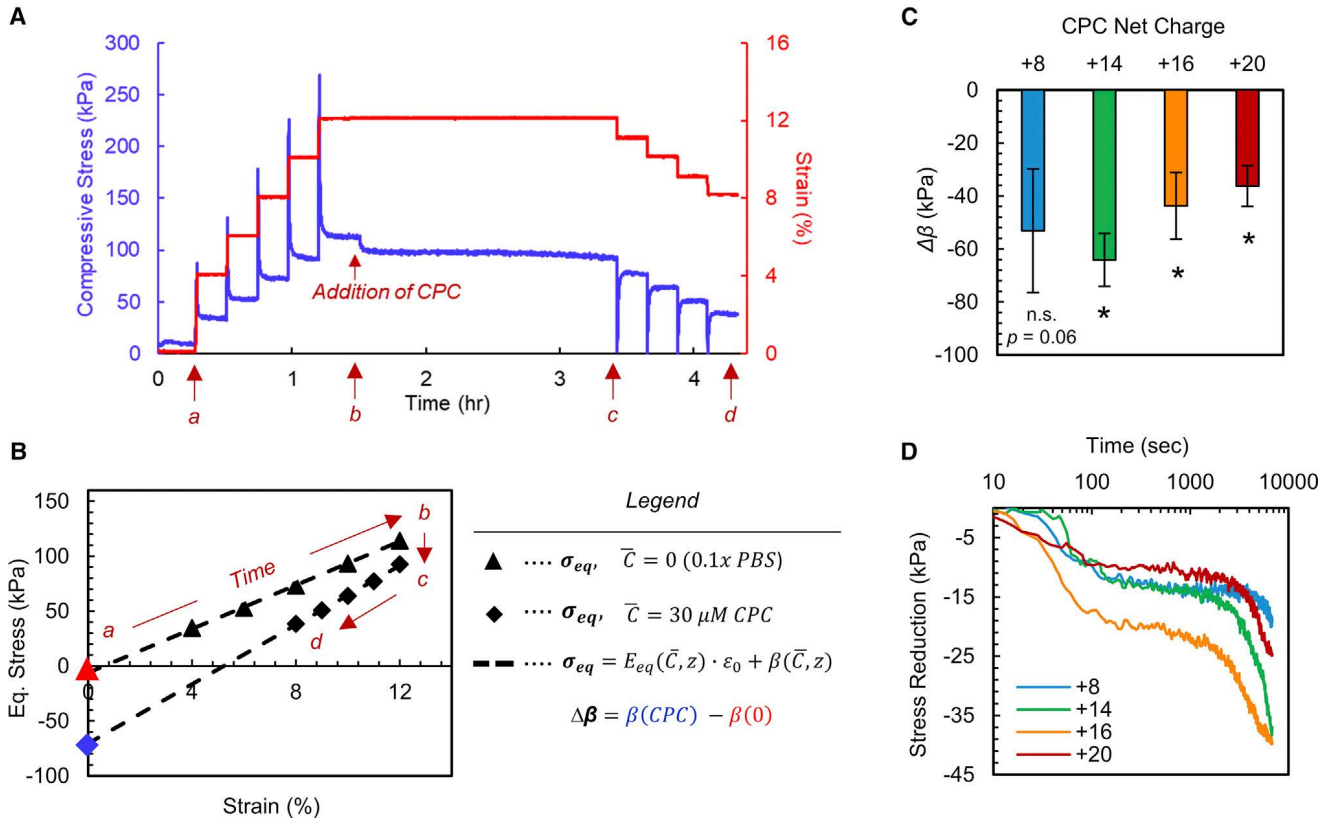

FIGURE 3 Real-time measurement of reduction in swelling stress during transient CPC uptake. (*A*) The testing process adapted from Eisenberg and Grodzinsky (36) was used to measure osmotic deswelling induced by CPC uptake. Following five stress-relaxation cycles in hypotonic saline (time $a \rightarrow b$), CPC was added to the testing bath, and constant strain was held for 2 h (time $b \rightarrow c$). After this period, stress relaxation was repeated (time $c \rightarrow d$). (*B*) The SLS model shown in Fig. 1 was fit to each stress-relaxation interval (before and after CPC treatment), and equilibrium stress was plotted against the corresponding strain level. Stress-strain data before and after CPC were fit to separate linear regression models (*dashed lines*). The net change in free swelling pressure ($\Delta\beta$) from CPC treatment was calculated as the difference in y-intercepts for the two stress-strain linear fits (i.e., difference in stress at $\varepsilon_0 = 0$; see *Legend*). (*C*) $\Delta\beta$ was quantified for explants treated with CPCs of each net charge level (+8 to +20). Data are plotted as means with error bars representing standard deviations. Statistical markers (*) represent $p \leq 0.05$, calculated by two-sided, paired t-test between swelling pressure before and after addition of CPC ($N = 3$–5 per condition). n.s., not significant. (*D*) Curves from representative samples depicting transient intra-tissue stress levels under constant 12% strain over 2 h of CPC uptake (beginning at $t = 0$). Stress reductions were calculated relative to the equilibrium stress at the point of CPC introduction for corresponding samples (at time b, following the fifth pre-CPC stress-relaxation interval).

Please cite this article in press as: Warren et al., Effects of polycationic drug carriers on the electromechanical and swelling properties of cartilage, Biophysical Journal (2022), https://doi.org/10.1016/j.bpj.2022.06.024

the transport profile of cationic drug carriers in cartilage. We observed a sharp drop in stress in the first ≈100 s after CPC was added to the bath, which is consistent with the phenomenon of Donnan partitioning (due to electrostatic interactions) inducing rapid entry of CPC at the tissue-bath interface at early times. After this period of rapid deswelling, the intra-tissue stress appeared to level until ≈1000 s. Previous studies with CPCs describe a similar temporal pattern of peptide transport through cartilage tissue whereby CPC uptake exhibits a lag period during which intra-tissue binding sites are occupied (9,12). Interestingly, previously measured lag times for intra-tissue transport are on the order of 1000 s, which is consistent with the pseudo-equilibration of CPC-induced stress reduction observed here (evident in Fig. 3 *D*). Finally, after ≈1000 s for all CPC charge variants, intra-tissue stress was reduced at a higher rate, which is also consistent with previous observations describing a steady-state flux of CPC into the tissue following occupation of all intra-tissue binding sites. Overall, given the consistency of the temporal pattern of stress reduction with previous transport studies, these results provide further evidence that deswelling is closely related to the amount of CPC in the tissue.

Carrier-induced tissue stiffening is mediated by electrostatic interactions between CPCs and the cartilage ECM

We next explored the mechanisms by which CPC-induced tissue stiffening occurs, as observed in tissues with healthy FCD (Fig. 1 *C*). To do so, we deconvoluted bulk modulus measurements into Donnan and non-Donnan components, under the assumption of a triphasic framework (see non-ideal Donnan modeling of osmotic swelling pressure). Since each component represents key macromolecular interactions within the tissue (i.e., charge shielding and macromolecular conformational entropy of the solid matrix for E_{eq}^{Donnan} and $E_{eq}^{Non-Donnan}$, respectively), we reasoned that detecting relative changes in separate modulus components induced by CPCs may provide mechanistic insight into the biophysical interactions underlying our earlier observations while measuring bulk moduli. Because E_{eq}^{Donnan} cannot be measured directly, we employed a theoretical non-ideal Donnan osmotic model to generate estimates, which could then be used to extrapolate $E_{eq}^{Non-Donnan}$ (see Eq. 11). Importantly, this model incorporates experimentally measurable parameters, including the intra-tissue CPC concentration $\overline{C}_{CPC}$, the FCD of the tissue ($\overline{C}_{FCD}$), and the salt concentration in the surrounding bath (C_0). This model was developed based on classical Donnan osmotic theory (30,52) and incorporates the counter charge introduced by CPCs in order to predict CPC-induced deswelling (23). Furthermore, to improve the accuracy of modeling predictions, we modified the ideal model previously described by our group to incorporate an empirical attenuation parameter ξ, which accounts for non-ideality(34). The model used herein is described further in non-ideal Donnan modeling of osmotic swelling pressure and Figs. S3 and S4, and is summarized in Fig. 4 *A*.

We began by implementing this model to estimate the electrostatic/Donnan moduli of the CPC-equilibrated explants previously analyzed by stress-relaxation testing (from Fig. 1). Using average uptake ratio measurements for each CPC variant, we calculated E_{eq}^{Donnan} for each CPC treatment condition, with both normal-FCD and 50% GAG-depleted tissues (shown in Fig. 4, *B* and *C*, respectively, in comparison with measured moduli). Overall, the Donnan modulus of both normal and GAG-depleted cartilage tissues was lower with CPC treatment compared with untreated control. The Donnan model estimates suggest that CPCs of higher net charge and uptake induce a larger reduction in E_{eq}^{Donnan}, which is consistent with our empirical observations of free swelling changes with CPC treatment (Fig. 3). Supported by our experimental deswelling measurements, these modeling results further suggest that CPCs can induce significant charge shielding, which manifests in decreased compressive stiffness of the tissue. Importantly, this modeling approach quantitatively demonstrates that non-negligible charge shielding likely occurred even in normal-FCD tissues, for which experimental measurements showed a contradictory net increase in bulk stiffness. This therefore provides further evidence that multiple CPC-matrix interactions simultaneously occurred at the nano scale, which had competing outcomes on measurable mechanical properties. For normal-FCD tissues, the electrostatic charge-shielding effects were evidently dominated by other, non-Donnan interactions, which result in a net increase in the tissue's stiffness.

The insights provided by deconvoluting bulk modulus measurements into Donnan and non-Donnan components prompted us to further investigate the mechanisms by which CPCs increase the stiffness of cartilage. We hypothesized that CPCs may participate in electrostatic binding with the GAG chains of matrix proteoglycans. Since CPCs are multivalent with charge distributed across the peptide length (estimated to be 3.5 nm as an α-helix, which is of the same length scale as the inter-GAG distance of cartilage (30)), binding mediated by electrostatic interactions could, in effect, physically link the ECM and increase stiffness. Notably, although this phenomenon involves charge interactions, this binding would be considered a non-Donnan effect because it influences the modulus of the solid phase of the tissue (i.e., its macromolecular ECM constituents).

To test whether the increase in stiffness associated with CPC uptake depends on electrostatic interactions, we measured the modulus of explants pre-equilibrated with CPC +14 with testing performed at multiple different salt concentrations (ranging from hypotonic to hypertonic). This experimental setup can be interpreted as a competitive binding experiment, since at hypertonic salinity the presence of overwhelming amounts of small cations (Na^+)

Please cite this article in press as: Warren et al., Effects of polycationic drug carriers on the electromechanical and swelling properties of cartilage, Biophysical Journal (2022), https://doi.org/10.1016/j.bpj.2022.06.024

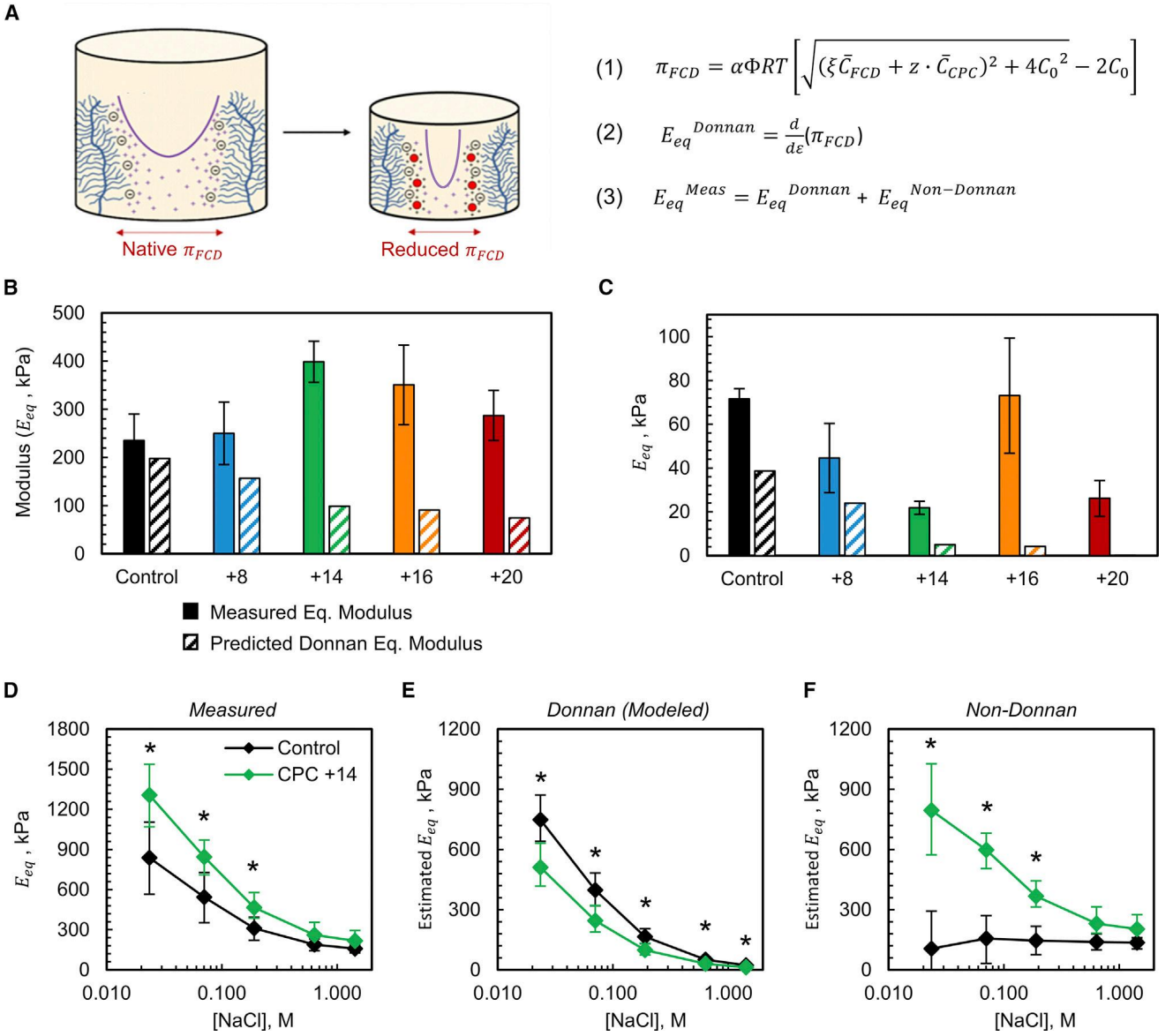

FIGURE 4 Quantification of CPC-induced changes in Donnan and non-Donnan components of the bulk equilibrium modulus of cartilage. (*A*) A non-ideal Donnan model for intra-cartilage osmotic swelling pressure was fit to experimental data and used to calculate electrostatic/Donnan modulus components (E_{eq}^{Donnan}) for individual samples, based on CPC net charge and uptake measurements (Eqs. 1 and 2) (shown in (*A*)). (*B* and *C*) Predicted Donnan moduli of normal-FCD and 50% GAG-depleted cartilage, respectively, following treatment with CPCs of varying net charge; E_{eq}^{Donnan} values are shown in comparison with measured moduli (E_{eq}^{Meas}) for corresponding CPC conditions at physiological salinity (from Fig. 1). (*D*) The equilibrium moduli of explants pre-equilibrated with CPC +14 were measured at varying levels of bath salinity to investigate the dependence of E_{eq} on charge interactions. Using the model and Eq. 3 shown in (*A*), equilibrium modulus measurements were deconvoluted into Donnan (*E*) and non-Donnan (*F*) components for each measured salinity level. Donnan moduli were calculated and averaged for individual explants using corresponding GAG and CPC uptake measurements and varying C_0 in Eq. 1 (shown in (*A*)); non-Donnan moduli were extrapolated from corresponding E_{eq}^{Meas} and E_{eq}^{Donnan} values for each explant using Eq. 3 (shown in (*A*)). Data are plotted as means with error bars representing 95% bootstrap confidence intervals. Statistical markers (*) represent $p \leq 0.05$, calculated by two-sided *t*-test, compared with control at corresponding [NaCl] levels. $N = 8$ per condition.

out-compete CPCs for electrostatic binding sites on the negatively charged matrix. Therefore, if CPC-induced stiffening is mediated by electrostatic interactions, we would expect the magnitude of the stiffness increase to depend closely on the surrounding salt concentration. Indeed, as shown in Fig. 4 *D*, the magnitude of the difference in modulus between control and CPC +14 explants increased with lower salt: the modulus of CPC +14 explants was 55.8% higher than the control at hypotonic salinity, whereas there was no statistically significant difference at salt concentrations higher than 0.6 M.

To further probe the effect of electrostatic binding, we utilized the non-ideal Donnan model to deconvolute bulk modulus measurements from this experiment into Donnan and non-Donnan components (shown in Fig. 4, *E* and *F*, respectively). Across all NaCl concentrations,

Please cite this article in press as: Warren et al., Effects of polycationic drug carriers on the electromechanical and swelling properties of cartilage, Biophysical Journal (2022), https://doi.org/10.1016/j.bpj.2022.06.024

the estimates of E_{eq}^{Donnan} generated by the model were lower for CPC +14-treated tissues compared with control, as expected due to charge shielding. Importantly, the extrapolated values for the non-Donnan modulus component clearly illustrate the dependence of CPC stiffening on electrostatic interactions: whereas $E_{eq}^{Non-Donnan}$ for control explants was constant across varying [NaCl] (a fundamental assumption of this analysis), $E_{eq}^{Non-Donnan}$ for CPC +14 explants exhibited a clear dependence on bath salinity (Fig. 4 *F*). An important feature of this relationship is that $E_{eq}^{Non-Donnan}$ for both untreated and CPC +14 explants were the same at salt concentrations greater than 0.6 M, demonstrating that charge interactions were necessary for the stiffening effect of CPCs to occur. Overall, these results provide strong evidence that the observed increase in stiffness of cartilage following CPC treatment was primarily mediated by electrostatic interactions between CPC molecules and the anionic tissue ECM.

ECM and chondrocyte health remained unaffected by CPC uptake

In addition to investigating mechanical changes associated with CPC uptake, this study aimed to evaluate whether such changes adversely affect tissue matrix and chondrocyte health. To do so, we utilized in vitro culture models of both live articular cartilage explants and free chondrocytes to measure the biological response to CPC exposure.

Cartilage explants were cultured with high concentrations of CPCs for 8 days to investigate the response of chondrocytes to CPC in situ. As shown in Fig. 5 *A*, treatment with CPCs +8 to +16 did not lead to increased cumulative GAG loss from the tissue compared with untreated control throughout the duration of culture. Interestingly, CPC +20 treatment resulted in a modest decrease in GAG loss at early time points. In contrast to CPCs of lower net charge, stronger electrostatic interactions with the matrix FCD hinder CPC +20 transport beyond the superficial ≈20% of tissue thickness (12). The uniquely observed lower GAG content measured in the surrounding media for CPC +20-treated tissues may therefore be attributable to steric hindrance from high concentrations of CPC in the superficial zone, which could block the flow of large proteoglycans/GAG chains out of the tissue.

Relative chondrocyte metabolic rate was measured using the alamarBlue assay at day 8 of culture, which revealed no change in cell metabolism induced by CPC treatment compared with control (Fig. 5 *B*). Furthermore, select explants were sectioned and stained for imaging of chondrocyte viability (Fig. 5 *C*). Some cell death was observed near the superficial zone of explants across conditions, although this may be attributable to cell death from slicing and explant punching (53). Nevertheless, chondrocytes remained largely viable across all CPC treatments, as indicated by the large visible proportion of green cells. Altogether, these results indicate that CPCs of all charges exhibited minimal adverse biological effects in cartilage explants.

Finally, to allow for direct quantification of CPC uptake within chondrocytes, we exposed primary bovine chondrocyte monolayers to 5 μM of each CPC variant (conjugated to FAM) for 1 h and analyzed the cells by flow cytometry. Gates defining healthy chondrocytes were set based on the forward scatter and side scatter of untreated chondrocytes, which were applied to chondrocytes from all CPC treatment groups (Fig. 5 *D*). Notably, nearly all cells analyzed fell within the preset healthy cell gate across treatment with each CPC variant (Fig. 5 *E*) despite high intracellular uptake of CPCs +14 to +20 (demonstrated quantitatively in Fig. 5 *F* and supported by imaging in Fig. 5 *G*), indicating few adverse effects to cell morphology. Altogether, this provides evidence that CPCs are non-cytotoxic to chondrocytes at the concentrations tested despite high cellular penetration.

DISCUSSION

Positively charged DDS are rapidly emerging as a promising modality that can enable therapeutically effective concentrations of disease-modifying drugs inside connective tissues with anionic charge, such as articular cartilage in the case of OA (3,4,7,8). In this study, we have evaluated the effects of arginine-rich CPCs on the mechanical properties and biological health of bovine articular cartilage. In doing so, we aimed to 1) measure the changes in the tissue's compressive stiffness associated with uptake of CPCs possessing various net charges (+8 to +20) and 2) elucidate the biophysical interactions between CPC molecules and macromolecular ECM constituents that mediate such changes. A mechanistic understanding of carrier-tissue interactions is of great importance for the design of future cationic DDS, since the extent of these potentially adverse effects may depend directly on tunable properties of the DDS, such as size and net charge (23).

We present three key findings that describe the impact of CPCs on cartilage biomechanics. First, we found that CPCs had contradictory effects on tissue explants with different FCD: while CPCs increased the compressive modulus of native cartilage with normal FCD, stiffness was decreased by CPCs in enzymatically GAG-depleted explants (Fig. 1). We observed that in both cases the magnitude of stiffening/softening correlated with the uptake of different CPC charge variants. This suggests that multiple distinct CPC-mediated biophysical phenomena occurred simultaneously within the tissue with opposite effects, and that the nature of the dominating interaction depended on the tissue's FCD. Considering these surprising contradictory observations, we next aimed to elucidate the mechanisms by which CPCs simultaneously stiffen and soften cartilage.

The second main finding of this study was that the transient uptake of CPCs directly induced osmotic deswelling

Please cite this article in press as: Warren et al., Effects of polycationic drug carriers on the electromechanical and swelling properties of cartilage, Biophysical Journal (2022), https://doi.org/10.1016/j.bpj.2022.06.024

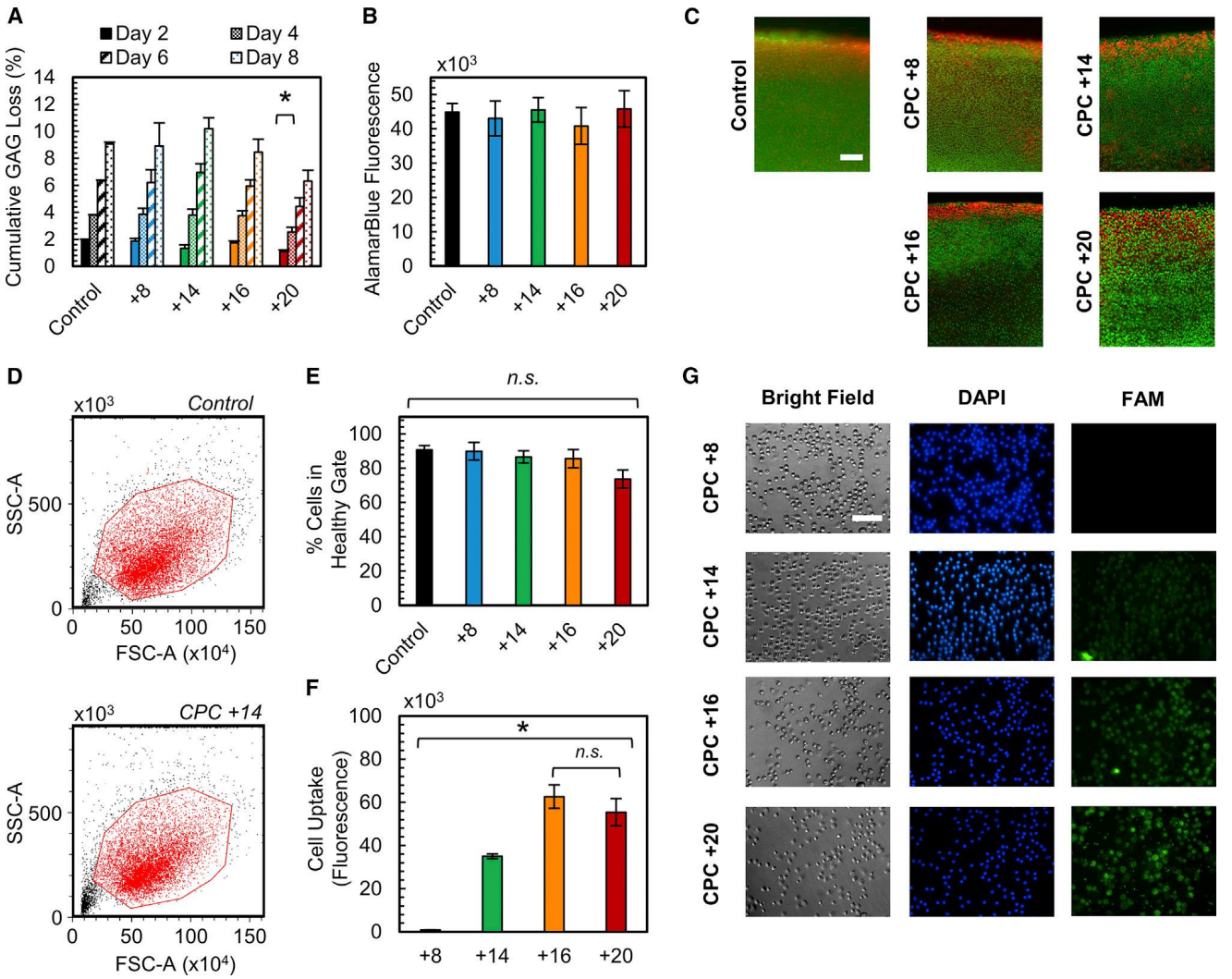

FIGURE 5 Evaluation of matrix proteoglycan integrity and chondrocyte health following CPC treatment using in vitro live tissue explant and chondrocyte culture models. (*A*) Cumulative GAG loss from explants to the surrounding medium over 8 days of culture, measured by DMMB assay. (*B*) Metabolism of chondrocytes in situ after 8 days of explant culture with 30 μM CPC treatment every 2 days, measured by AlamarBlue assay. Statistical marker (*) in (*A*) represents $p \leq 0.05$ compared with control, $N = 3$ explants per condition. (*C*) Live-dead staining of chondrocytes in tissues treated with CPCs, taken on day 8 of culture. Viable cells are stained green and non-viable cells are stained red. Scale bar represents 200 μm. (*D*) Chondrocytes were cultured with 5 μM CPC for 1 h and subsequently analyzed by flow cytometry. Representative gating of control and CPC +14-treated chondrocytes. FSC-A, forward scatter area; SSC-A, side scatter area. (*E*) Proportion of chondrocytes that fell within the predesignated healthy cell gate following exposure to CPCs of varying net charge. (*F*) Relative uptake of FAM-labeled CPCs into chondrocytes, measured by flow cytometry. Statistical marker (*) represents $p \leq 0.05$ compared with CPC +14 (10,000 events for each sample). n.s., not significant. (*G*) Representative images showing uptake and retention of FAM-labeled CPCs within chondrocytes following fixing and washing with PBS. Scale bar represents 50 μm. All data are plotted as means with error bars representing standard deviations.

in cartilage by shielding like-charge repulsions between anionic matrix GAGs (36). We measured reductions in free swelling pressure between 36.3 and 64.2 kPa resulting from CPC uptake, and these magnitudes are consistent with our previously reported predictions of CPC-induced deswelling obtained by a Donnan osmotic model (23) (Fig. S5). Additionally, the temporal profile of deswelling was consistent with previously described intra-cartilage transport properties of CPCs (9,12), suggesting a correlation between uptake and deswelling. Most notably, the reduction in tissue stress upon the addition of CPC was initially rapid (<100 s) but subsequently reached a pseudo-equilibrium until $\approx$1000 s, which is consistent with the observation that cationic nanocarriers exhibit an initial lag period in uptake on the order of 1000 s as intra-tissue binding sites are occupied. Therefore, the results presented here provide direct evidence in support of the hypothesis proposed by our group (23) and others (22) that cationic drug carriers can shield repulsive electrostatic forces within cartilage.

A technical limitation of our deswelling experiments was that measurements were conducted with hypotonic (0.01 M) PBS, which was chosen so that the overall magnitudes of

Please cite this article in press as: Warren et al., Effects of polycationic drug carriers on the electromechanical and swelling properties of cartilage, Biophysical Journal (2022), https://doi.org/10.1016/j.bpj.2022.06.024

swelling pressures were large enough to be measured above the noise floor of the mechanical testing machine. Furthermore, it should be noted that the CPC uptake period was only 2 h, which is shorter than the time required for equilibration of intra-tissue transport (38). While the testing setup used was adequate to test the hypothesis that CPCs induce osmotic deswelling in a proof-of-concept sense, the noted limitations force violation of fundamental assumptions of the modeling approach used here, such as spatial homogeneity of CPC uptake, since these 3 kDa CPCs only penetrate the superficial edge of cartilage in a 2-h time span (12). Thus, the ability to relate our direct measurements of deswelling to other equilibrium mechanical properties of CPC-treated cartilage is limited. Nevertheless, these results have strong implications for the design of future cationic DDS intended for delivery to a variety of electrically charged tissues (5): since cationic carriers can alter the swelling properties of the target tissue, constraints on tolerable levels of tissue deswelling must be imposed, which in turn necessitates careful consideration of the net charge and dosing of these therapeutics. Notably, we present here the first use (to our knowledge) of the experimental methodology and theoretical model described by Eisenberg and Grodzinsky for measuring osmotic swelling pressures, applied in the context of DDS. We envision that these methods will be refined by further studies and become a crucial component of the development and evaluation processes for cationic DDS.

We next investigated the biophysical interactions by which CPC-induced stiffening occurs. The third key finding presented here is that the magnitude of CPC-induced stiffening (ΔE_{eq}) in healthy cartilage explants was dependent on the salinity of the fluid immersing the tissue during testing. While ΔE_{eq} was amplified at hypotonic compared with physiological salinity, there was no statistically significant change in modulus when measured with a hypertonic bathing solution (Fig. 4). This observation provides important insight into the mechanism of CPC-induced stiffening, demonstrating that electrostatic interactions between CPCs and constituents of the solid ECM are necessary for stiffening to occur. This effect is further illustrated by using the Donnan model of CPC-induced charge shielding to deconvolute bulk modulus measurements into Donnan and non-Donnan components: while $E_{eq}^{Non-Donnan}$ for control explants was constant across different bath salinities (as expected), $E_{eq}^{Non-Donnan}$ for CPC-treated tissues showed clear amplification at hypotonic salinity. Using the Donnan model to separate measurements of the bulk modulus into triphasic components represents a novel analysis technique, which may be highly valuable as a screening tool in future drug carrier design. There are multiple limitations with using both ideal (23,30) and non-ideal Donnan models (34), including the assumption of homogeneous distribution of CPC within the tissue. Notably, we tested multiple variations (an ideal model and two variations of the non-ideal model; see supporting material), each of which yielded similar results in modeling $E_{eq}^{Non-Donnan}$ and demonstrated the dependence of $E_{eq}^{Non-Donnan}$ on bath salinity for CPC explants (Fig. S4). Future work should focus on improving this modeling approach to incorporate the variable spatial distribution of carriers in different cartilage zones, as well as accounting for the physical orientation of a cationic DDS in the brush network of proteoglycans, which would enable application of nanoscale models such as the Poisson-Boltzmann cell (30,54). This proof-of-concept analysis supplements direct measurements and provides further strong evidence for the central role of electrostatic interactions underlying the observed carrier-induced stiffening effect.

The results presented here allow us to propose a novel model that describes the carrier-ECM interactions responsible for measurable changes in bulk, equilibrium mechanical properties of a target tissue. As depicted in Fig. 6, the intention of this theory is to relate tunable properties of cationic DDS, such as net charge, size, or spatial charge distribution, to specific biophysical interactions that result in downstream alterations to the tissue's mechanical homeostasis. As such, we envision that this model can help guide the design of cationic DDS by introducing new considerations for their physical properties. As a demonstration of its use, our methodology of deconvoluting measurements of the bulk tissue modulus into Donnan and non-Donnan components represents a quantitative application of this model. This is because experimentally monitoring relative changes in the modulus components can elucidate the relative contributions of the physical interactions depicted in Fig. 6 on net changes to bulk material properties.

In light of triphasic theory (27,55), we denote two broad classes of phenomena that may occur simultaneously within the tissue and possibly induce competing effects. These phenomena are defined by the triphasic component of the tissue that is affected by the carrier, represented quantitatively by either the Donnan or non-Donnan component of the compressive modulus. First, as demonstrated empirically herein, shielding of like-charge repulsions between neighboring GAG chains by high interstitial concentrations of cationic DDS will induce osmotic deswelling and decrease the bulk stiffness of the tissue (via diminished $E_{eq}^{Non-Donnan}$). This is an especially crucial consideration for delivery to already degenerated tissue that has a reduced FCD (56), such as arthritic cartilage (as demonstrated in Fig. 1 and predicted previously by Warren and Bajpayee (23)). From a design standpoint, higher amounts of counter charge within the target tissue will enhance the charge-shielding effect; as such, limitations may need to be imposed on a carrier's net charge or dosing.

Next, in addition to charge shielding, the current study has elucidated a previously unknown stiffening effect induced by cationic DDS, which increases $E_{eq}^{Non-Donnan}$. We envision that

Please cite this article in press as: Warren et al., Effects of polycationic drug carriers on the electromechanical and swelling properties of cartilage, Biophysical Journal (2022), https://doi.org/10.1016/j.bpj.2022.06.024

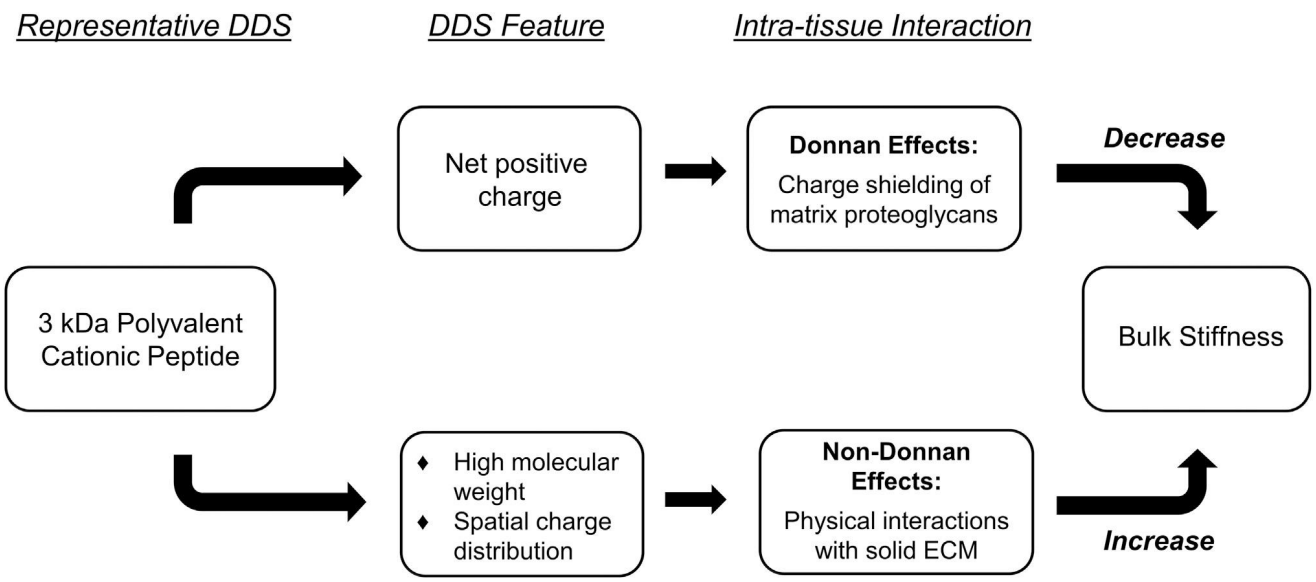

FIGURE 6 Proposed model for biophysical interactions between cationic drug-delivery systems (DDS) and negatively charged constituents of a tissue's extracellular matrix (ECM), which can alter the macroscale mechanical properties of the tissue. The data presented herein suggest multiple effects of CPCs on the mechanical properties of cartilage. First, the high amount of positive counter charge introduced into the tissue space by these carriers results in shielding of like-charge repulsions between neighboring proteoglycan GAG chains. This manifests in reduced osmotic swelling pressure within the tissue as well as a lower bulk compressive modulus. Second, the macromolecular size and spatial distribution of multivalent charge possessed by many cationic carriers facilitates physical interactions with the solid ECM, which increase the bulk compressive stiffness of the tissue. For example, electrostatic binding between the carrier and multiple proteoglycans may induce a physical linking effect, and high amounts of mass within the tissue from macromolecular carriers can result in blocked nanopores and hindered interstitial fluid flow. Thus, from a design perspective, the mechanical "side effects" of cationic carriers that depend on tunable properties (i.e., charge, size, spatial charge distribution) may be dichotomized into two broad categories based on the tissue phase affected: Donnan, influencing the like-charge repulsions that give rise to tissue swelling; and non-Donnan, altering the mechanical properties of the solid components of the ECM (which may or may not involve electrostatic binding).

stiffening may occur by multiple mechanisms depending on the carrier. For instance, this may involve attractive binding interactions with ECM macromolecules (12,57), in which case the spatial separation of charged moieties is a crucial design parameter that can directly influence the degree of matrix physical linkages. Additionally, another potential non-Donnan effect is that conformational entropy of the solid matrix upon compression may be impeded by high amounts of exogenous mass introduced into the tissue interstitium. Under non-equilibrium loading, this would manifest in hindered interstitial fluid flow and increased pressurization due to blocked nanopores (29), which is consistent with our observation of decreased permeability by CPCs (Fig. 1). In this case, the carrier's size would directly correlate with enhanced stiffening. In general, by this proposed theory, the Donnan and non-Donnan phenomena would have competing effects on the bulk stiffness of the tissue, and the relative contributions of each would largely depend on the carrier itself and the FCD of the target tissue, warranting individual experimental characterization of different DDS. Notably, the results presented here do not repudiate the possibility for synergy between these phenomena. Theoretically, deswelling of the tissue may bring macromolecular matrix fibers closer together and reduce the tissue's pore size, which could enhance solid matrix interactions; this effect should be studied further. This model can be a valuable tool in the design of cationic DDS intended for applications in a wide range of connective tissue diseases.

While these results provide strong evidence that stiffening was mediated by electrostatic interactions between CPCs and macromolecules of the solid ECM, the nature of this interaction is unclear, including which ECM components interacted with CPCs (i.e., collagen or GAGs) and how such interactions conferred macroscale stiffening. We propose that CPCs can participate in physical linkages with the solid cartilage matrix and that enhanced interconnectivity of the ECM is responsible for the concomitant increase in stiffness. Matrix crosslinking is a well-defined phenomenon that is known to augment the mechanical properties of tissues (58) and gel systems (59,60). For instance, many studies have described the clinical application of covalent crosslinking of collagen fibers to stabilize a variety of connective tissue allografts, including cartilage (43,61,62), tendons (63,64), meniscus (65), the intervertebral disk (66,67), and the eye (68). In fact, previous studies that induced collagen crosslinking via glutaraldehyde in cartilage (62) and triglycidyl amine in meniscus (65) reported magnitudes of stiffening roughly similar to the observations reported here with CPCs (twofold and 32% increases in modulus, respectively). Given the size of CPC molecules in relation to the average pore size of cartilage ($\approx$3.5 nm versus 6 nm pores (9,69)), we envision that

Please cite this article in press as: Warren et al., Effects of polycationic drug carriers on the electromechanical and swelling properties of cartilage, Biophysical Journal (2022), https://doi.org/10.1016/j.bpj.2022.06.024

CPC-matrix linkages may take three forms (which could in theory occur simultaneously): intra-fiber linking of collagen molecules (58,61), linking of neighboring GAG chains (59), and linkages between GAG chains and constituents of a neighboring collagen fiber. Each of these phenomena would be mediated by non-covalent binding forces (H-bonding, hydrophobic) and, primarily, electrostatic attractions.

CPCs may have induced matrix stiffening via intra-fiber collagen linking in a mechanism similar to previously studied exogenous crosslinking agents, such as genipin and glutaraldehyde (70). Although this may have contributed to the increase in modulus observed here, multiple lines of evidence strongly suggest that GAG chains are involved in the dominant CPC-matrix interaction responsible for macroscale stiffening. First, the net effect of CPCs in GAG-depleted explants was softening by charge shielding, indicating that the ECM stiffening effect was severely diminished in these tissues compared with explants with healthy FCD. Since GAG-depleted explants have roughly the same collagen content as healthy tissues, it is unlikely that the dominant physical linking mechanism by CPCs involved only collagen fibers. Furthermore, given the polyelectrolyte nature of both CPCs and GAG chains, it is intuitive that electrostatic attractions between the two species would confer stability to the matrix (59). In fact, in an analogous mechanism, such inter-polyelectrolyte attractive forces have been leveraged extensively as a crosslinking strategy for stabilization of chitosan-chondroitin sulfate gel systems (71–73). Further studies of the nature of binding between CPCs and individual constituents of the cartilage ECM, including measurements and comparison of binding affinities, are required for full characterization of the carrier-induced stiffening effect reported here. We note that such mechanistic studies of binding interactions with the ECM of a target tissue should be applied to the development of any future cationic DDS. Especially because we observed stiffening with a DDS as small as CPCs, larger constructs such as nanoparticles (19,74) (on the order of the cartilage pore size or larger) may exhibit markedly higher stiffening effects. This stiffening may be severe enough to require amelioration by supplementing the DDS with secondary treatments that block carrier-matrix binding, and thorough knowledge of the specific interactions between the carrier and matrix constituents would be crucial for the design of such therapeutics.

A secondary aim of this study was to empirically evaluate CPCs as a clinically translatable delivery system for OA therapeutics. To this end, we characterized the biocompatibility and cytotoxicity (24,75) of high CPC concentrations using in vitro chondrocyte and cartilage explant culture models (39,43). The results of biological studies (shown in Fig. 5) indicate that CPC treatment did not adversely affect chondrocyte viability or metabolic rate, nor did CPCs exacerbate matrix degeneration as measured by GAG loss. Such an in vitro screen is an important evaluative step before progression to in vivo studies, and the results promote the safety of CPCs as a biocompatible delivery system. Additionally, an important corollary to our finding that CPCs themselves did not adversely affect chondrocyte health is that the mechanical changes in the ECM associated with CPCs, demonstrated here, were also tolerated by chondrocytes. The biological results allow us to propose biocompatible limits to levels of carrier-induced deswelling (76), since the measured levels of deswelling ($\approx$10–100 kPa) and ECM stiffening ($\approx$50%) evidently did not stress chondrocytes to the point of affecting viability or metabolism. Further studies investigating the dose-dependent mechanical and biological response of cartilage to CPC (and other cationic DDS) treatment are warranted. Imposition of upper limits to biologically tolerable levels of swelling and stiffness changes are a crucial consideration in the design of future cationic delivery systems for tissues that rely on swelling for functionality (5,77). Moreover, considering their biocompatibility, the mechanical effects of deswelling and ECM stiffening described here may impart CPCs with intrinsic therapeutic potential, which can be leveraged in multiple contexts. For example, the charge-shielding capacity of CPCs or another highly cationic DDS may be useful for treating pathologies involving tissue swelling pressures, such as reducing intra-ocular pressure in glaucoma patients (78). Additionally, CPCs could be repurposed as a transient, non-covalent stabilizing agent for connective tissue allografts, similar to genipin (58) and glutaraldehyde (62). Finally, the observation that CPC +20 reduced GAG loss in vitro at early time points (Fig. 5 *A*) suggests that CPC-proteoglycan binding interactions may mediate increased integrity of proteoglycan assemblies (and intermediate aggrecan structures (79)) beyond aggrecan-hyaluronan association (80); therefore, CPCs could be used to improve intra-tissue proteoglycan retention. Leveraging the mechanical effects of cationic DDS while simultaneously maintaining tissue biocompatibility should be the subject of further studies.

There are multiple limitations to the mechanical testing and modeling methods used here that are worth noting. First, representing cartilage as a solid, linear viscoelastic material is inadequate to fully describe the poroelastic characteristics of the tissue (44,45). An important consequence of the use of the SLS model is that the hydraulic permeability values presented are only estimates; applying a poroelastic model to the stress-relaxation data obtained here would yield more accurate measurements. However, the purpose of this study was not to characterize the structural material properties of CPC-equilibrated cartilage with the highest possible degree of accuracy. Rather, we primarily aimed to assess the relative changes in bulk material properties (i.e., modulus) induced by different CPC charge variants, from which mechanistic insights into carrier-ECM biophysical interactions could be derived. Therefore, we believe that the stress-relaxation tests and associated viscoelastic

modeling performed here were an adequate screening method to elucidate bulk mechanical changes induced by CPCs and compare the effects of charge variants. Nevertheless, deeper analysis of the mechanical data obtained herein using a poroelastic model (44,45) is warranted, which could provide improved accuracy for the measured mechanical parameters as well as finer granularity to the comparisons between CPCs. Additionally, it is important to note that time-dependent mechanics in cartilage can arise from both fluid flow and flow-independent intrinsic viscoelasticity from friction between ECM macromolecules. In the context of the current study, it is difficult to delineate the dominating contributor, given that the magnitudes of measured time constants (50–100 s, Fig. S2) were higher than previously reported solid matrix relaxation times ($\approx$1 s (81)). Therefore, our results suggest that CPCs may alter time-dependent mechanics through either 1) hindering interstitial fluid flow or 2) increasing intermolecular friction of ECM components.

Many of the analyses presented here assumed that the spatial distribution of CPCs throughout the tissue was homogeneous. Multiple studies have shown that cationic nanocarriers exhibit variable rates of penetration through the superficial and deep zones of cartilage (9,12) and other charged tissues (82). Given the variation in the FCD (and by extension, mechanical properties) of cartilage with depth (29), CPCs and other charged constructs may exhibit markedly enhanced deswelling and/or stiffening effects in different zones of the tissue. This is likely especially true for trypsin-treated cartilage: local diffusivities of solute transport have been shown to closely correlate with spatially variable FCD induced by enzymatic matrix degradation (83), which would further confound the spatial heterogeneity of concentration-dependent mechanical effects of CPCs measured here. From a clinical perspective, accumulation of CPCs in the superficial zone at sites of arthritic lesions may lead to locally enhanced adverse mechanical side effects, which could further exacerbate tissue degradation originating at these points through disproportionate compaction. These phenomena highlight the necessity for further studies of the relative effects of cationic carriers and their associated mechanical effects in the different zones of cartilage tissue.

CONCLUSIONS

In summary, we have provided direct evidence that macromolecular, cationic drug nanocarriers can alter the mechanical homeostasis of cartilage tissue by multiple mechanisms. Using CPCs as a tunable experimental system, our results demonstrate stark changes in tissue stiffness and hydraulic permeability resulting from treatment. The effects of CPCs were contradictory depending on the tissue's FCD, with CPCs inducing stiffening in healthy cartilage explants and decreasing the modulus of 50% GAG-depleted tissues. This may be explained by the simultaneous occurrence of multiple competing mechanical effects induced by CPCs as demonstrated here, including charge shielding/osmotic deswelling and electrostatic binding with the ECM. We propose a model that relates the biophysical interactions between a cationic drug carrier and the target tissue's ECM to the carrier's physical, tunable properties, and we envision that this theory can be a useful tool to guide the design of future cationic DDS. Future studies should focus on further characterization of the specific binding interactions that mediate ECM stiffening, improvement of the deswelling measurement technique described here, more accurate modeling of charge shielding for improved deconvolution of modulus measurements into Donnan and non-Donnan components, and consideration of the local effects of variable interstitial concentrations of CPCs in different zones of cartilage tissue.

SUPPORTING MATERIAL

Supporting material can be found online at https://doi.org/10.1016/j.bpj.2022.06.024.

AUTHOR CONTRIBUTIONS

M.R.W. designed the study, conducted experiments, developed computational tools for data analysis, performed data analysis, interpreted data, created figures, and wrote and edited the manuscript. A.V. conducted experiments, created figures, and interpreted data. S.B. conducted experiments and interpreted data. A.G.B. obtained funding, conceived and designed the study, interpreted data, and wrote and edited the manuscript/figures. All authors reviewed and approved the manuscript prior to submission.

ACKNOWLEDGMENTS

This study was supported by NSF CAREER award #2141841, the National Institute of Health (NIH) R01 grant AR075121, and NIH Trailblazer R21 grant EB028385. We would like to thank Dr. Shikhar Mehta and Vishrudan Swami for their assistance in running experiments.

DECLARATION OF INTERESTS

The authors declare no competing interests.

REFERENCES

1. Huebner, K. D., N. G. Shrive, and C. B. Frank. 2014. Dexamethasone inhibits inflammation and cartilage damage in a new model of post-traumatic osteoarthritis. *J. Orthop. Res.* 32:566–572. https://doi.org/10.1002/jor.22568. https://www.ncbi.nlm.nih.gov/pubmed/24375646.
2. Hunter, D. J., M. C. Pike, …, T. McAlindon. 2010. Phase 1 safety and tolerability study of BMP-7 in symptomatic knee osteoarthritis. *BMC Musculoskelet. Disord.* 11:232. https://doi.org/10.1186/1471-2474-11-232.
3. Bajpayee, A. G., and A. J. Grodzinsky. 2017. Cartilage-targeting drug delivery: can electrostatic interactions help? *Nat. Rev. Rheumatol.* 13:183–193. https://doi.org/10.1038/nrrheum.2016.210. https://www.ncbi.nlm.nih.gov/pubmed/28202920.
4. Mehta, S., T. He, and A. G. Bajpayee. 2021. Recent advances in targeted drug delivery for treatment of osteoarthritis. *Curr. Opin. Rheumatol.*

33:94–109. https://doi.org/10.1097/BOR.0000000000000761. https://www.ncbi.nlm.nih.gov/pubmed/33229973.

5. Vedadghavami, A., C. Zhang, and A. G. Bajpayee. 2020. Overcoming negatively charged tissue barriers: drug delivery using cationic peptides and proteins. *Nano Today.* 34:100898. https://doi.org/10.1016/j.nantod.2020.100898. https://www.ncbi.nlm.nih.gov/pubmed/32802145.
6. Bhosale, A. M., and J. B. Richardson. 2008. Articular cartilage: structure, injuries and review of management. *Br. Med. Bull.* 87:77–95. https://doi.org/10.1093/bmb/ldn025. https://www.ncbi.nlm.nih.gov/pubmed/18676397.
7. Young, C. C., A. Vedadghavami, and A. G. Bajpayee. 2020. Bioelectricity for drug delivery: the promise of cationic therapeutics. *Bioelectricity.* 2:68–81. https://doi.org/10.1089/bioe.2020.0012. https://www.ncbi.nlm.nih.gov/pubmed/32803148.
8. Kumar, S., and B. Sharma. 2020. Leveraging electrostatic interactions for drug delivery to the joint. *Bioelectricity.* 2:82–100. https://doi.org/10.1089/bioe.2020.0014. https://www.ncbi.nlm.nih.gov/pubmed/32856016.
9. Bajpayee, A. G., C. R. Wong, …, A. J. Grodzinsky. 2014. Avidin as a model for charge driven transport into cartilage and drug delivery for treating early stage post-traumatic osteoarthritis. *Biomaterials.* 35:538–549. https://doi.org/10.1016/j.biomaterials.2013.09.091. https://www.ncbi.nlm.nih.gov/pubmed/24120044.
10. Bajpayee, A. G., M. Scheu, …, R. M. Porter. 2014. Electrostatic interactions enable rapid penetration, enhanced uptake and retention of intra-articular injected avidin in rat knee joints. *J. Orthop. Res.* 32:1044–1051. https://doi.org/10.1002/jor.22630. https://www.ncbi.nlm.nih.gov/pubmed/24753019.
11. Bajpayee, A. G., M. A. Quadir, …, A. J. Grodzinsky. 2016. Charge based intra-cartilage delivery of single dose dexamethasone using Avidin nano-carriers suppresses cytokine-induced catabolism long term. *Osteoarthritis Cartilage.* 24:71–81. https://doi.org/10.1016/j.joca.2015.07.010. https://www.ncbi.nlm.nih.gov/pubmed/26211608.
12. Vedadghavami, A., E. K. Wagner, …, A. G. Bajpayee. 2019. Cartilage penetrating cationic peptide carriers for applications in drug delivery to avascular negatively charged tissues. *Acta Biomater.* 93:258–269. https://doi.org/10.1016/j.actbio.2018.12.004. https://www.ncbi.nlm.nih.gov/pubmed/30529083.
13. Cook Sangar, M. L., E. J. Girard, …, J. M. Olson. 2020. A potent peptide-steroid conjugate accumulates in cartilage and reverses arthritis without evidence of systemic corticosteroid exposure. *Sci. Transl. Med.* 12:eaay1041. https://doi.org/10.1126/scitranslmed.aay1041.
14. Krishnan, Y., H. A. Rees, …, A. J. Grodzinsky. 2018. Green fluorescent proteins engineered for cartilage-targeted drug delivery: insights for transport into highly charged avascular tissues. *Biomaterials.* 183:218–233. https://doi.org/10.1016/j.biomaterials.2018.08.050. https://www.ncbi.nlm.nih.gov/pubmed/30173104.
15. DiDomenico, C. D., and L. J. Bonassar. 2018. The effect of charge and mechanical loading on antibody diffusion through the articular surface of cartilage. *J. Biomech. Eng.* https://doi.org/10.1115/1.4041768. https://www.ncbi.nlm.nih.gov/pubmed/30347103.
16. DiDomenico, C. D., Z. Xiang Wang, and L. J. Bonassar. 2017. Cyclic mechanical loading enhances transport of antibodies into articular cartilage. *J. Biomech. Eng.* 139. https://doi.org/10.1115/1.4035265. https://www.ncbi.nlm.nih.gov/pubmed/27893039.
17. He, T., I. Shaw, …, A. G. Bajpayee. 2022. Single-dose intra-cartilage delivery of kartogenin using a cationic multi-arm avidin nanocarrier suppresses cytokine-induced osteoarthritis-related catabolism. *Cartilage.* 13:194760352210930. https://doi.org/10.1177/19476035221093072. https://www.ncbi.nlm.nih.gov/pubmed/35491681.
18. He, T., C. Zhang, …, A. G. Bajpayee. 2020. Multi-arm Avidin nanoconstruct for intra-cartilage delivery of small molecule drugs. *J. Control. Release.* 318:109–123. https://doi.org/10.1016/j.jconrel.2019.12.020. https://www.ncbi.nlm.nih.gov/pubmed/31843642.
19. Perni, S., and P. Prokopovich. 2017. Poly-beta-amino-esters nano-vehicles based drug delivery system for cartilage. *Nanomedicine.* 13:539–548. https://doi.org/10.1016/j.nano.2016.10.001. https://www.ncbi.nlm.nih.gov/pubmed/27746232.
20. Geiger, B. C., S. Wang, …, P. T. Hammond. 2018. Cartilage-penetrating nanocarriers improve delivery and efficacy of growth factor treatment of osteoarthritis. *Sci. Transl. Med.* 10:eaat8800. https://doi.org/10.1126/scitranslmed.aat8800.
21. Brown, S., J. Pistiner, …, B. Sharma. 2019. Nanoparticle properties for delivery to cartilage: the implications of disease state, synovial fluid, and off-target uptake. *Mol. Pharm.* 16:469–479. https://doi.org/10.1021/acs.molpharmaceut.7b00484. https://www.ncbi.nlm.nih.gov/pubmed/28669194.
22. Young, W. T. 2016. Cartilage Stress Relaxation Induced by Intra-tissue Transport of Cationic Nanoparticles : Implications for Post-traumatic Osteoarthritis Drug Delivery. Massachusetts Institute of Technology. Department of Mechanical Engineering. Massachusetts Institute of Technology.
23. Warren, M. R., and A. G. Bajpayee. 2021. Modeling electrostatic charge shielding induced by cationic drug carriers in articular cartilage using Donnan osmotic theory. *Bioelectricity.* https://doi.org/10.1089/bioe.2021.0026.
24. Verdurmen, W. P., and R. Brock. 2011. Biological responses towards cationic peptides and drug carriers. *Trends Pharmacol. Sci.* 32:116–124. https://doi.org/10.1016/j.tips.2010.11.005. https://www.ncbi.nlm.nih.gov/pubmed/21167610.
25. Lu, X. L., and V. C. Mow. 2008. Biomechanics of articular cartilage and determination of material properties. *Med. Sci. Sports Exerc.* 40:193–199. https://doi.org/10.1249/mss.0b013e31815cb1fc. https://www.ncbi.nlm.nih.gov/pubmed/18202585.
26. Mow, V. C. G., M. Gibbs, …, A. Athanasiou. 1989. Biphasic indentation of articular cartilage-II. A numerical algorithm and an experimental study. *J. Biomech.* 22:853–861. https://doi.org/10.1016/0021-9290(89)90069-9.
27. Lai, W. M., J. S. Hou, and V. C. Mow. 1991. A triphasic theory for the swelling and deformation behaviors of articular cartilage. *J. Biomech. Eng.* 113:245–258. https://doi.org/10.1115/1.2894880.
28. Ehrlich, S., N. Wolff, …, C. P. Winlove. 1998. The osmotic pressure of chondroitin sulphate solutions: experimental measurements and theoretical analysis. *Biorheology.* 35:383–397. https://doi.org/10.1016/s0006-355x(99)80018-3.
29. Maroudas, A., and P. Bullough. 1968. Permeability of articular cartilage. *Nature.* 219:1260–1261. https://doi.org/10.1038/2191260a0.
30. Buschmann, M. D. G., and A. J. Grodzinsky. 1995. A molecular model of proteoglycan-associated electrostatic forces in cartilage mechanics. *J. Biomech. Eng.* 117:179–192. https://doi.org/10.1115/1.2796000.
31. Han, E. H., S. S. Chen, …, R. Sah. 2011. Contribution of proteoglycan osmotic swelling pressure to the compressive properties of articular cartilage. *Biophys. J.* 101:916–924. https://doi.org/10.1016/j.bpj.2011.07.006. https://www.ncbi.nlm.nih.gov/pubmed/21843483.
32. Canal Guterl, C., C. T. Hung, and G. A. Ateshian. 2010. Electrostatic and non-electrostatic contributions of proteoglycans to the compressive equilibrium modulus of bovine articular cartilage. *J. Biomech.* 43:1343–1350. https://doi.org/10.1016/j.jbiomech.2010.01.021. https://www.ncbi.nlm.nih.gov/pubmed/20189179.
33. Maroudas, A. 1976. Balance between swelling pressure and collagen tension in normal and degenerate cartilage. *Nature.* 260:808–809. https://doi.org/10.1038/260808a0.
34. Zimmerman, B. K., R. J. Nims, …, G. A. Ateshian. 2021. Direct osmotic pressure measurements in articular cartilage demonstrate non-ideal and concentration-dependent phenomena. *J. Biomech. Eng.* 143:041007. https://doi.org/10.1115/1.4049158. https://www.ncbi.nlm.nih.gov/pubmed/33210125.
35. Maroudas, A. 1968. Physicochemical properties of cartilage in the light of ion exchange theory. *Biophys. J.* 8:575–595. https://doi.org/10.1016/s0006-3495(68)86509-9.
36. Eisenberg, S. R., and A. J. Grodzinsky. 1985. Swelling of articular cartilage and other connective tissues: electromechanochemical forces. *J. Orthop. Res.* 3:148–159. https://doi.org/10.1002/jor.1100030204.
37. Parsons, J. R., and J. Black. 1979. Mechanical behavior of articular cartilage : quantitative changes with alteration of ionic environment.

J. Biomech. 12:765–773. https://doi.org/10.1016/0021-9290(79)90162-3.

38. Vedadghavami, A., S. Mehta, and A. G. Bajpayee. 2020. Characterization of intra-cartilage transport properties of cationic peptide carriers. *J. Vis. Exp.* https://doi.org/10.3791/61340. https://www.ncbi.nlm.nih.gov/pubmed/32831304.

39. Mehta, S., S. Akhtar, …, A. G. Bajpayee. 2019. Interleukin-1 receptor antagonist (IL-1Ra) is more effective in suppressing cytokine-induced catabolism in cartilage-synovium co-culture than in cartilage monoculture. *Arthritis Res. Ther.* 21:238. https://doi.org/10.1186/s13075-019-2003-y. https://www.ncbi.nlm.nih.gov/pubmed/31722745.

40. Farndale, R. W. S., C. A. Sayers, and A. J. Barrett. 1982. A direct spectrophotometric microassay for sulfated glycosaminoglycans in cartilage cultures. *Connect. Tissue Res.* 9:247–248.

41. Bajpayee, A. G., R. E. De la Vega, …, R. M. Porter. 2017. Sustained intra-cartilage delivery of low dose dexamethasone using a cationic carrier for treatment of post traumatic osteoarthritis. *Eur. Cell Mater.* 34:341–364. https://doi.org/10.22203/eCM.v034a21. https://www.ncbi.nlm.nih.gov/pubmed/29205258.

42. Soltz, M. A. A., and G. A. Ateshian. 2000. Interstitial fluid pressurization during confined compression cyclical loading of articular cartilage. *Ann. Biomed. Eng.* 28:150–159. https://doi.org/10.1114/1.239.

43. Mehta, S., C. C. Young, …, A. G. Bajpayee. 2021. Resveratrol and curcumin attenuate ex vivo sugar-induced cartilage glycation, stiffening, senescence, and degeneration. *Cartilage.* 13:1214S–1228S. https://doi.org/10.1177/1947603520988768. https://www.ncbi.nlm.nih.gov/pubmed/33472415.

44. Armstrong, C. G. L., W. M. Lai, and V. C. Mow. 1984. An analysis of the unconfined compression of articular cartilage. *J. Biomech. Eng.* 106:165–173. https://doi.org/10.1115/1.3138475.

45. Grodzinsky, A. J. 2011. Fields, Forces, and Flows in Biological System. Garland Science.

46. Manning, G. S. 1969. Limiting laws and counterion condensation in polyelectrolyte solutions I. Colligative properties. *J. Chem. Phys.* 51:924–933. https://doi.org/10.1063/1.1672157.

47. Manning, G. S. 2007. Counterion condensation on charged spheres, cylinders, and planes. *J. Phys. Chem.* 111:8554–8559. https://doi.org/10.1021/jp0670844.

48. He, T., B. Li, T. Colombani, …, A. G. Bajpayee. 2021. Hyaluronic acid-based shape-memory cryogel scaffolds for focal cartilage defect repair. *Tissue Eng. Part A.* 27:748–760. https://doi.org/10.1089/ten.TEA.2020.0264. https://www.ncbi.nlm.nih.gov/pubmed/33108972.

49. Orloff, J., and J. Bloom. 2014. 18-05 Introduction to Probability and Statistics. Spring. Massachusetts Institute of Technology: MIT OpenCouseWare. License: Creative Commons BY-NC-SA. https://ocw.mit.edu/.

50. Lyyra, T., J. P. A. Arokoski, …, A. Vihko. 1999. Experimental validation of arthroscopic cartilage stiffness measurement using enzymatically degraded cartilage samples. *Phys. Med. Biol.* 44:525–535. https://doi.org/10.1088/0031-9155/44/2/017.

51. Bonassar, L. J., K. A. Jeffries, …, A. J. Grodzinsky. 1995. In vivo effects of stromelysin on the composition and physical properties of rabbit articular cartilage in the presence and absence of a synthetic inhibitor. *Arthritis Rheum.* 38:1678–1686. https://doi.org/10.1002/art.1780381121.

52. Basser, P. J., and A. J. Grodzinsky. 1993. The Donnan model derived from microstructure. *Biophys. Chem.* 46:57–68. https://doi.org/10.1016/0301-4622(93)87007-j.

53. Redman, S. N. D., G. Dowthwaite, …, C. W. Archer. 2004. The cellular responses of articular cartilage to sharp and blunt trauma. *Osteoarthritis Cartilage.* 12:106–116. https://doi.org/10.1016/j.joca.2002.12.001.

54. Dean, D., J. Seog, …, A. J. Grodzinsky. 2003. Molecular-level theoretical model for electrostatic interactions within polyelectrolyte brushes: applications to charged glycosaminoglycans. *Langmuir.* 19:5526–5539. https://doi.org/10.1021/la027001k.

55. Grodzinsky, A. J., V. Roth, …, V. C. Mow. 1981. The significance of electromechanical and osmotic forces in the nonequilibrium swelling behavior of articular cartilage in tension. *J. Biomech. Eng.* 103:221–231. https://doi.org/10.1115/1.3138284.

56. Poulet, B. 2017. Models to define the stages of articular cartilage degradation in osteoarthritis development. *Int. J. Exp. Pathol.* 98:120–126. https://doi.org/10.1111/iep.12230. https://www.ncbi.nlm.nih.gov/pubmed/28585282.

57. Naik, R. J., R. Sharma, …, M. Ganguli. 2015. Exogenous chondroitin sulfate glycosaminoglycan associate with arginine-rich peptide-DNA complexes to alter their intracellular processing and gene delivery efficiency. *Biochim. Biophys. Acta.* 1848:1053–1064. https://doi.org/10.1016/j.bbamem.2015.01.012. https://www.ncbi.nlm.nih.gov/pubmed/25637297.

58. Wang, Z., H. Liu, …, X. Yang. 2020. Regeneration of skeletal system with genipin crosslinked biomaterials. *J. Tissue Eng.* 11:2041731420974861. https://doi.org/10.1177/2041731420974861. https://www.ncbi.nlm.nih.gov/pubmed/33294154.

59. Alvarez-Lorenzo, C., B. Blanco-Fernandez, …, A. Concheiro. 2013. Crosslinked ionic polysaccharides for stimuli-sensitive drug delivery. *Adv. Drug Deliv. Rev.* 65:1148–1171. https://doi.org/10.1016/j.addr.2013.04.016. https://www.ncbi.nlm.nih.gov/pubmed/23639519.

60. Yan, S., T. Wang, …, J. Yin. 2014. Injectable in situ self-cross-linking hydrogels based on poly(L-glutamic acid) and alginate for cartilage tissue engineering. *Biomacromolecules.* 15:4495–4508. https://doi.org/10.1021/bm501313t. https://www.ncbi.nlm.nih.gov/pubmed/25279766.

61. Pinheiro, A., A. Cooley, …, S. Elder. 2016. Comparison of natural crosslinking agents for the stabilization of xenogenic articular cartilage. *J. Orthop. Res.* 34:1037–1046. https://doi.org/10.1002/jor.23121. https://www.ncbi.nlm.nih.gov/pubmed/26632206.

62. Oungoulian, S. R., K. E. Hehir, …, G. A. Ateshian. 2014. Effect of glutaraldehyde fixation on the frictional response of immature bovine articular cartilage explants. *J. Biomech.* 47:694–701. https://doi.org/10.1016/j.jbiomech.2013.11.043. https://www.ncbi.nlm.nih.gov/pubmed/24332617.

63. Fessel, G., C. Gerber, and J. G. Snedeker. 2012. Potential of collagen cross-linking therapies to mediate tendon mechanical properties. *J. Shoulder Elbow Surg.* 21:209–217. https://doi.org/10.1016/j.jse.2011.10.002. https://www.ncbi.nlm.nih.gov/pubmed/22244064.

64. Ng, K. W., F. Wanivenhaus, …, S. A. Maher. 2013. Differential cross-linking and radio-protective effects of genipin on mature bovine and human patella tendons. *Cell Tissue Bank.* 14:21–32. https://doi.org/10.1007/s10561-012-9295-3. https://www.ncbi.nlm.nih.gov/pubmed/22350064.

65. Hunter, S. A., H. S. Rapoport, …, R. J. Levy. 2010. Biomechanical and biologic effects of meniscus stabilization using triglycidyl amine. *J. Biomed. Mater. Res. A.* 93:235–242. https://doi.org/10.1002/jbm.a.32523. https://www.ncbi.nlm.nih.gov/pubmed/19557790.

66. Hedman, T. P., W. P. Chen, …, S. Y. Chuang. 2017. Effects of collagen crosslink augmentation on mechanism of compressive load sharing in intervertebral discs. *J. Med. Biol. Eng.* 37:94–101. https://doi.org/10.1007/s40846-016-0207-z. https://www.ncbi.nlm.nih.gov/pubmed/30416413.

67. Yerramalli, C. S., A. I. Chou, …, D. M. Elliott. 2007. The effect of nucleus pulposus crosslinking and glycosaminoglycan degradation on disc mechanical function. *Biomech. Model. Mechanobiol.* 6:13–20. https://doi.org/10.1007/s10237-006-0043-0. https://www.ncbi.nlm.nih.gov/pubmed/16715318.

68. Zhang, Y., A. H. Conrad, and G. W. Conrad. 2011. Effects of ultraviolet-A and riboflavin on the interaction of collagen and proteoglycans during corneal cross-linking. *J. Biol. Chem.* 286:13011–13022. https://doi.org/10.1074/jbc.M110.169813. https://www.ncbi.nlm.nih.gov/pubmed/21335557.

69. DiDomenico, C. D., M. Lintz, and L. J. Bonassar. 2018. Molecular transport in articular cartilage - what have we learned from the past 50 years? *Nat. Rev. Rheumatol.* 14:393–403. https://doi.org/10.1038/s41584-018-0033-5. https://www.ncbi.nlm.nih.gov/pubmed/29899547.

70. McGann, M. E., C. M. Bonitsky, …, D. R. Wagner. 2015. Genipin crosslinking of cartilage enhances resistance to biochemical degradation and

mechanical wear. *J. Orthop. Res.* 33:1571–1579. https://doi.org/10.1002/jor.22939. https://www.ncbi.nlm.nih.gov/pubmed/25939430.

71. Sui, W., L. Huang, …, Q. Bo. 2008. Preparation and properties of chitosan chondroitin sulfate complex microcapsules. *Colloids Surf. B Biointerfaces.* 65:69–73. https://doi.org/10.1016/j.colsurfb.2008.02.022. https://www.ncbi.nlm.nih.gov/pubmed/18440788.

72. Fajardo, A. R., L. C. Lopes, …, E. C. Muniz. 2011. Effect of stoichiometry and pH on the structure and properties of Chitosan/Chondroitin sulfate complexes. *Colloid Polym. Sci.* 289:1739–1748. https://doi.org/10.1007/s00396-011-2497-6.

73. Fajardo, A. R., S. L. Fávaro, …, E. C. Muniz. 2013. Dual-network hydrogels based on chemically and physically crosslinked chitosan/chondroitin sulfate. *Reactive Funct. Polym.* 73:1662–1671. https://doi.org/10.1016/j.reactfunctpolym.2013.10.003.

74. Melgar-Asensio, I., I. Kandela, …, J. Henkin. 2018. Extended intravitreal rabbit eye residence of nanoparticles conjugated with cationic arginine peptides for intraocular drug delivery: in vivo imaging. *Invest. Ophthalmol. Vis. Sci.* 59:4071–4081. https://doi.org/10.1167/iovs.18-24087. https://www.ncbi.nlm.nih.gov/pubmed/30098194.

75. Kilk, K., R. Mahlapuu, …, Ü. Langel. 2009. Analysis of in vitro toxicity of five cell-penetrating peptides by metabolic profiling. *Toxicology.* 265:87–95. https://doi.org/10.1016/j.tox.2009.09.016. https://www.ncbi.nlm.nih.gov/pubmed/19799958.

76. Amin, A. K., J. S. Huntley, …, A. C. Hall. 2008. Osmolarity influences chondrocyte death in wounded articular cartilage. *J. Bone Joint Surg. Am.* 90:1531–1542. https://doi.org/10.2106/JBJS.G.00857. https://www.ncbi.nlm.nih.gov/pubmed/18594103.

77. Bush, P. G., and A. C. Hall. 2005. Passive osmotic properties of in situ human articular chondrocytes within non-degenerate and degenerate cartilage. *J. Cell Physiol.* 204:309–319. https://doi.org/10.1002/jcp.20294. https://www.ncbi.nlm.nih.gov/pubmed/15668989.

78. Schuster, A. K., C. Erb, …, N. Pfeiffer. 2020. The diagnosis and treatment of glaucoma. *Dtsch. Arztebl. Int.* 117:225–234. https://doi.org/10.3238/arztebl.2020.0225. https://www.ncbi.nlm.nih.gov/pubmed/32343668.

79. Bayliss, M. T., S. Howat, …, J. Dudhia. 2000. The organization of aggrecan in human articular cartilage. *J. Biol. Chem.* 275:6321–6327. https://doi.org/10.1074/jbc.275.9.6321. https://www.ncbi.nlm.nih.gov/pubmed/10692431.

80. Han, B., Q. Li, …, L. Han. 2019. Decorin regulates the aggrecan network integrity and biomechanical functions of cartilage extracellular matrix. *ACS Nano.* 13:11320–11333. https://doi.org/10.1021/acsnano.9b04477. https://www.ncbi.nlm.nih.gov/pubmed/31550133.

81. June, R. K., S. Ly, and D. P. Fyhrie. 2009. Cartilage stress-relaxation proceeds slower at higher compressive strains. *Arch. Biochem. Biophys.* 483:75–80. https://doi.org/10.1016/j.abb.2008.11.029. https://www.ncbi.nlm.nih.gov/pubmed/19111671.

82. Wagner, E. K., A. Vedadghavami, …, A. G. Bajpayee. 2020. Avidin grafted dextran nanostructure enables a month-long intra-discal retention. *Sci. Rep.* 10:12017. https://doi.org/10.1038/s41598-020-68351-1. https://www.ncbi.nlm.nih.gov/pubmed/32694557.

83. DiDomenico, C. D., A. Kaghazchi, and L. J. Bonassar. 2019. Measurement of local diffusion and composition in degraded articular cartilage reveals the unique role of surface structure in controlling macromolecular transport. *J. Biomech.* 82:38–45. https://doi.org/10.1016/j.jbiomech.2018.10.019. https://www.ncbi.nlm.nih.gov/pubmed/30385000.